Hydroponic Container Farms: Validation of a Building Energy Model and its Integration in Urban Design

by

Mariana Liebman-Peláez

B.S. Mechanical Engineering
Tufts University, 2014

Submitted to the Department of Architecture
in Partial Fulfillment of the Requirements for the Degree of

Master of Science in Building Technology
at the
Massachusetts Institute of Technology

September 2020

Signature of Author: _____
Department of Architecture
August 7, 2020

Certified by: _____
Christoph Reinhart
Professor of Building Technology
Thesis Supervisor

Accepted by: _____
Leslie K. Norford
Professor of Building Technology
Chair, Department Committee on Graduate Students

Committee

Thesis Supervisor

Christoph Reinhart, PhD
Professor of Building Technology

Thesis Reader

Leslie K. Norford, PhD
Professor of Building Technology

Hydroponic Container Farms: Validation of a Building Energy Model and its Integration in Urban Design

by

Mariana Liebman-Peláez

Submitted to the Department of Architecture on August 7, 2020 in Partial Fulfillment of the Requirements for the Degree of Master of Science in Building Technology

Abstract

Controlled environment agriculture (CEA) systems, or plant factories, have developed within the urban context following efforts to expand local food production and provide an alternative to conventional agriculture with lower rates of greenhouse gas emissions and resource consumption. One urban CEA system, container farms, consist of vertical hydroponic farms inside retrofitted shipping containers. The artificially controlled interior environments within container farms along with their portability and modularity allow container farms to grow food in a variety of otherwise unused locations regardless of climate and daylight availability. While container farms and plant factories in general may provide a promising option for sustainable urban agriculture, they are highly energy intensive, particularly for lighting and thermal control. As a result, urban designers and policy makers require holistic assessment tools and methodologies to understand the viability of plant factories in reducing the greenhouse gas emissions of food systems. However, due to limitations of building performance simulation (BPS) tools, existing urban design methodologies assess the energy use of plant factories using simplified building energy models that omit the energetic effects of plants. While previous studies have developed methods that consider plant-air interactions within BPS tools through the use of co-simulators, to date there has been a lack of energy validation studies for such models.

This research attempts to bridge this gap by validating a first-principle hourly energy model for an operational hydroponic container farm located in Boston, Massachusetts. The energy model (NMBE of 3% and CV[RMSE]of 9%) combines a plant evapotranspiration model in parallel with a BPS tool, EnergyPlus. The validation focuses on the reliability of the energy model in predicting hourly conditioning loads and comments on the practical challenges and limitations of modeling hourly conditioning for container farms and other plant factories. Second, this research uses the validated energy model to simulate methods for reducing conditioning loads of container farms under various climate and upgrade scenarios. Finally, this research explores the integration of container farms in an urban neighborhood and the potential for reducing additional demands on the neighborhood's energy supply system.

Thesis Supervisor: Christoph Reinhart
Title: Professor of Building Technology

Contents

Acknowledgements

The completion of this thesis marks the end of two years full of growth, learning, and community. I am standing on the other side of this journey feeling immense gratitude for each step and every person along the way.

First, to Christoph, thank you for everything. Your constant support and trust has both pushed me and lifted me when I needed it. You have held me to high standards while being compassionate and so patient. Thank you always for your guidance and grounded perspectives that have often reminded me to think critically and practically. Most of all, thank you for welcoming me and everyone into this community and always spreading your good humor and optimism. It has been a privilege and a joy to learn from you and work with you.

To Les, thank you for your constant dedication and generosity to this community and your genuine interest in learning with your students. Thank you for the many conversations about energy balances, for taking the time and care to review this thesis, and always reminding me to be thorough and rigorous in my work.

To John, this thesis as is would not have been possible without you. Thank you for carefully collecting and monitoring all the data, for always checking in on me and providing guidance, for the countless hours deliberating about COP calculations, averaging scripts, plant energy balances... the list continues. You are an inspiring colleague and a wonderful person.

To Khadija, thank you sharing your love of plants, food, and sustainable agriculture. Over the past two years, I have learned so much from you. You have inspired me greatly with the care you put into your work and your persistent attention to detail.

This project would not have been possible without the generous support of the Center for Complex Engineering Systems in collaboration with King Abdulaziz City for Science & Technology (KACST). Thank you to all for this opportunity and for supporting me in this journey.

To all BT students, faculty, and staff, these two years have been that much more enriching and fun thanks to the wonderful and supportive people in this community. I have been so inspired by all of you and am forever grateful for the friendships I have made during my time here. Thank you to Nicole, Sam, and Zach for all your input and laughter behind the scenes of this thesis.

Finally, to all my friends and family, I feel so privileged and lucky to have you in my life. Whether or not you know it, each one of you has, in a way, been part of my growth over these past two years. To Angela, thank you for teaching me to be the best version of myself, to look ahead and work hard, and to keep my head steady on my shoulders. To my dear brother Alex, you were there at the start of this and all adventures. You inspire me always with the genuine way you live your life, with your integrity and curiosity, your spontaneous humor. Thank you for sharing this journey with me. To my parents, words cannot contain the gratitude I have for you both, for the boundless love and support, for the laughter and the grounding, for the role models and teachers you are to me each in your individual way. Gracias.

List of Acronyms

ACH	Air Changes per Hour
ASHRAE	American Society of Heating, Refrigerating and Air-Conditioning Engineers
BIA	Building Integrated Agriculture
BPS	Building Performance Simulation
CAC	Cultivation Area Cover
CEA	Controlled Environment Agriculture
CF	Container Farm
COP	Coefficient of Performance
CV(RMSE)	Coefficient of Variation of Root Mean Squared Error
DB	Dry-bulb
DP	Dew Point
EER	Energy Efficiency Ratio
EPW	EnergyPlus Weather Format
HPCF	Hyde Park Container Farm
HVAC	Heating, Ventilation, and Air Conditioning
LAI	Leaf Area Index
LED	Light Emitting Diode
NMBE	Normalized Mean Bias Error
PAR	Photosynthetically Active Radiation
PPFD	Photosynthetic Photon Flux Density
RH	Relative Humidity
SEER	Seasonal Energy Efficiency Ratio
TMY3	Typical Meteorological Year 3

List of Figures

List of Tables

1 Introduction

As cities and urban areas strive towards a sustainable future, the focus of carbon emission-reduction efforts is largely centered on cities' electricity supply, buildings, and transportation infrastructure [1]. This focus is consistent with the high percentage of emissions in urban areas produced by the building and transportation sectors. For example, in Boston MA, building and transportation sectors (including industrial buildings) account for nearly all city emissions at 71% and 29%, respectively [2]. However, such production-based emissions inventories omit the emissions associated with the consumption of goods by those living in urban areas. Additionally, as cities reduce emissions associated with physical infrastructure, emissions reductions from other sectors, as well as consumption-based sources, gain relevance.

Of growing interest is the incorporation of the emissions of food systems within assessments of overall urban emissions, for instance in [3] and [4]. This is driven in part by estimates that food systems account for 19-29% of global anthropogenic carbon emissions [5]. As arable land continues to decrease in availability on a global scale [6], urban designers and policy makers are further motivated to consider alternatives to conventional agriculture that not only reduce environmental impacts (with lower rates of land degradation, greenhouse gas emissions, and resource consumption), but that are also more resilient to changing climate conditions. A recent and ongoing debate is whether commercial urban agriculture can serve as a method for reducing emissions of urban areas [7]–[9]. For urban designers and policy makers, the question is whether commercial urban agriculture can reduce overall carbon emissions of cities in such a way that is economically feasible. To answer this question, it is necessary to understand the extent to which commercial urban agriculture can supply cities with food and the emissions associated with this alternative form of production.

Recent studies have shown that with dense, high-yield crop production, it would be possible to meet demands of urban vegetable consumption within the footprints of global urban areas [10]. This dense, high-yield crop production is best accomplished through controlled environment agriculture (CEA) systems, otherwise known as plant factories, which are soilless indoor farms with opaque walls and ceiling, fully artificial lighting, and fully active climate control for temperature, humidity, and carbon dioxide concentrations [11]. Compared to open-field agriculture, plant factories can yield more than 100 times the annual crop productivity per unit area [12]. Furthermore, the hydroponics systems commonly used in plant factories consume significantly less water per unit of crop yield as seen in one study where,

on average, hydroponics systems consumed 66 times less water compared to conventional agriculture [13]. Additionally, studies such as [14] have found that plant factories produce higher crop yields compared to greenhouses.

As reviewed by [15], CEA systems within or on the built environment, known as building integrated agriculture (BIA), fall into two typologies: vertical farms (buildings dedicated solely or in part to CEA), and container farms (standalone plant factories within shipping containers). While vertical farms have been widely considered for commercial urban agriculture, there has been a recent growth in interest in container farms [16]. Like all plant factories, the controlled interior environments within container farms with regard to temperature, humidity, water supply, and light allow container farms to grow food in a variety of locations regardless of climate and daylight availability. However, container farms have the added benefit of being modular, low-cost, readily available, and easy to transport. Additionally, container farms can be stacked, further increasing the yield per unit area of the systems [17]. While vertical farms within buildings would require the use of valuable urban real estate, shipping container farms have the option of temporarily or permanently occupying unused urban spaces. A similar concept has been previously seen in the use of repurposed shipping containers for modular data centers [18]. Furthermore, shipping containers have shown promise as modular systems for architectural applications [19]. Several companies actively develop container farms including Cropbox, Freight Farms, Modular Farms, and Square Roots.

While plant factories show promise in meeting urban vegetable demand while being synergistic with the urban fabric of a city, the question remains whether plant factories can reduce overall urban carbon emissions. Compared to open-field agriculture, plant factories can reduce emissions associated with land use, water consumption, pesticides, fertilizers, cultivation, and transport [16]. However, due to their artificial interior environments, plant factories are highly energy intensive, particularly for lighting and climate control. This creates the potential for plant factories to increase rather than decrease emissions compared to other forms of agriculture. For example, one study compared greenhouses and container farms in cities with varying climates and found that although crop yields were comparable in both systems, container farms were more energy intensive and the question of whether they ultimately reduced carbon emissions depended on local climate and existing food supply systems [20].

In response to the aforementioned potential and uncertainty regarding the viability of implementing plant factories, [15] identified a need for tools and methodologies for the holistic assessment of the environmental and economic impacts of such systems within urban contexts. An example of such a

methodology was developed by [21] and later implemented in a software tool, “Harvest” [22]. This methodology combines a building energy model and plant growth model to quantify the resource use efficiency of plant factories in energy inputs per unit of crop yield (kWh/kg). Such metrics, particularly the energy demands of plant factories, are of great interest to cities, plant factory owners, and grid utility companies. For cities concerned with emission reduction goals, input energy requirements of plant factories are readily translated into carbon emissions that can be weighed against the carbon emissions of conventional agriculture. For owners of plant factories, the ability to predict kWh/kg at the annual level is fundamental in planning for operating costs and understanding the potential for revenue. Furthermore, as the energy requirements of an urban area scale with the capacity of plant factories, utility companies become increasingly concerned with accurately quantifying the energy consumption of the plant factories at the hourly timescale. In particular, hourly plant factory loads and conditions that cause peaks in energy demand are necessary to understand the effects the additional load would have on future electric grid capacity.

One key component of such analyses are the building energy models used to predict the energy demands of plant factories. While building energy models for greenhouses have been widely studied and developed [23], [24], such models have not been validated for plant factories that have relatively larger internal gains and limited interaction with the exterior environment [14]. As noted by [25], defining the latent and sensible energy exchanges between plants and the closed interior environments is fundamental to such models. However, previously developed methods such as [21] for the holistic assessment of plant factories within urban contexts are based on simplified building energy models that omit the energetic effects of plants within plant factory environments. This is in part because existing building performance simulation (BPS) tools lack the components to explicitly represent the added complexity of plant evapotranspiration [26]. Previous studies have worked around this limitation by developing methods that consider plant-air interactions within BPS tools through the use of parallel models or co-simulators [14], [26]–[29]. The co-simulator model (DesignBuilder, EnergyPlus) used by [14] was validated for evapotranspiration rates of plants. Nevertheless, to the knowledge of the authors, no such methods that combine BPS tools with plant evapotranspiration models have been validated for the energy consumption of a plant factory.

In this research, we have attempted to bridge this gap by validating an hourly energy model for hydroponic container farm in compliance with [30]. The model used in this study following similar methods to [14], [26]–[29] to combine a plant evapotranspiration model with a BPS tool (EnergyPlus). The validation focuses on the reliability of the energy model in predicting hourly conditioning loads.

While lighting and equipment dominate the energy loads of plant factories, these are predictable and less variable in comparison to heating, ventilation and air conditioning (HVAC) energy demands. Furthermore, the validated energy model was used to create a template for a generic container farm that could be readily used in feasibility assessments of plant factories.

This thesis presents the results of energy measurements taken of an operational plant factory, a hydroponic container farm located in Boston, Massachusetts (MA), from August 2018 to July 2019. The research presented in this thesis consists of three parts. First, this research uses energy measurements of the container farm to produce a validated first-principle energy model. The validation study also comments on practical challenges and limitations of modeling hourly conditioning and total energy for container farms and other plant factories. The next two components of this research use the validated energy model to explore two areas of analyses that would be of interest to cities and urban designers, owners of plant factories, and utility companies. The second component of this research uses the validated energy model to simulate methods for reducing conditioning loads of container farms under various climate and upgrade scenarios. Finally, this research explores the integration of container farms in an urban neighborhood and the potential for reducing additional demands on the neighborhood's energy supply system.

2 Methods

This research consisted of three stages, each of which is described in the three sub-sections below. Section 2.1 describes the process of creating and validating an energy model for a container farm. This was done by developing an energy simulation in EnergyPlus, using the simulation to predict the energy loads of the container farm, and validating these results against measured energy consumption data. Section 2.2 describes the process of using the validated energy model from Section 2.1 to develop an energy model for a template container farm. The Section further describes how the template container farm energy model was used to estimate the hourly and total energy consumption of a template container farm for several climate and system modification scenarios. Section 2.3 describes the methodology used to explore the integration of template container farms in an urban neighborhood in Boston, Massachusetts and predict how these template container farms would affect the neighborhood's energy demand profile.

2.1 Energy Model Validation Methods

This Section describes the methods used in creating and validating a physics-based energy model for a container farm. Section 2.1.1 introduces the container farm used in this research while Section 2.1.2 reviews the theoretical background of the energy model. Sections 2.1.3 through 2.1.6 describe the steps taken to create and validate the hydroponic container farm energy model: collect the necessary data for the energy model and validation (2.1.3); define and run the energy model in EnergyPlus (2.1.4); calculate hourly coefficient of performance (COP) values for post-processing of the energy model results (2.1.5); and validate the energy model results against measured energy consumption data (2.1.6).

2.1.1 Hydroponic Container Farm Description

The energy model for this research was based on an existing hydroponic container farm operated by Freight Farms, a container farm design and manufacturing company located in Boston, MA. This container farm, referred to as the "Hyde Park container farm" (HPCF), was operational throughout the study from August 2018 through July 2019 in the production of leafy greens. The farm produced butterhead lettuce until the end of 2018 and, beginning in 2019, produced an assortment of leafy greens. The HPCF was constructed out of a retired refrigerated 40-foot shipping container within which Freight Farms installed a vertical hydroponics system and a custom climate-control system. Figure 1 and Figure 2 depict the HPCF in relation to its physical surroundings as well as the major components of' the hydroponics and climate control systems.

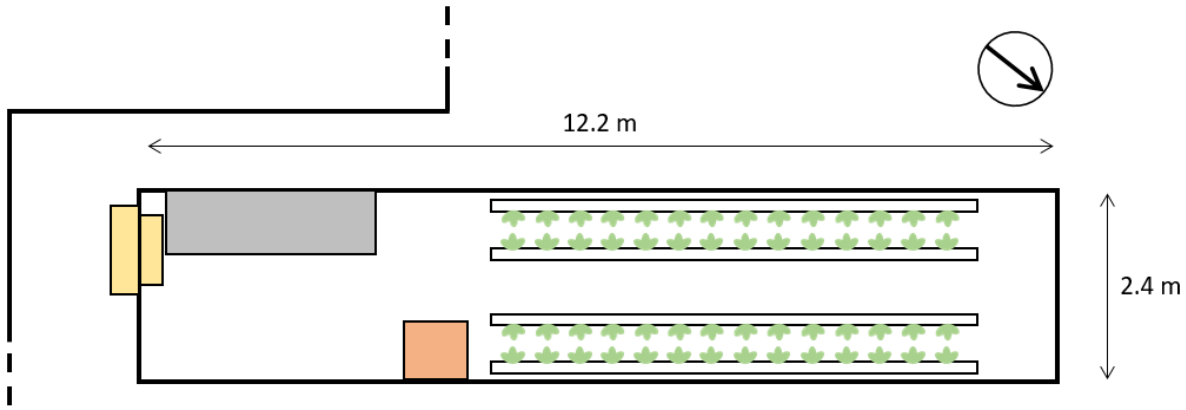

Figure 1: Top view of the HPCF in relation to neighboring building.

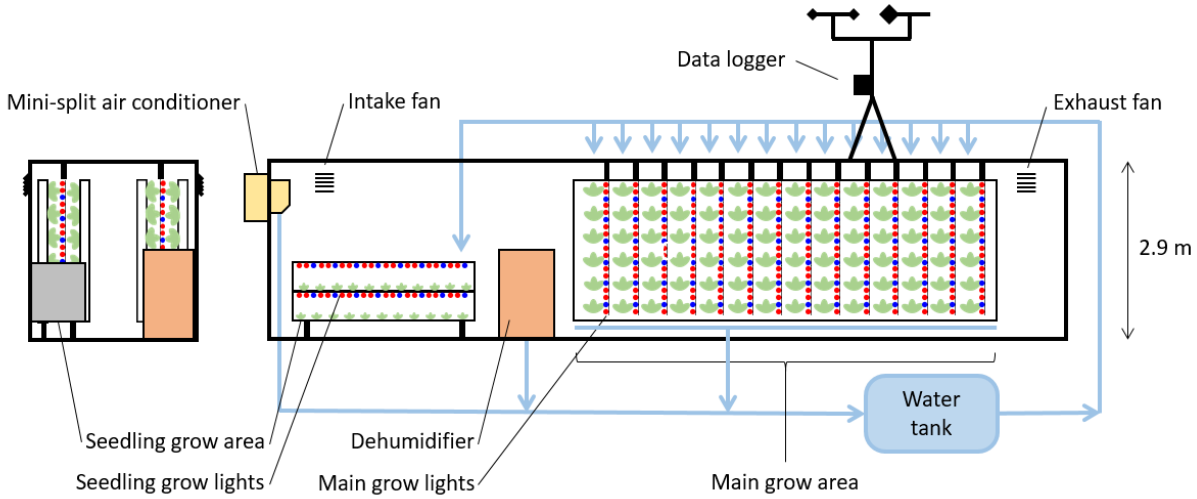

Figure 2: Left (left) and front (right) views of the HPCF and major system components.

2.1.2 Energy Model Theory

The energy balance in Equation 1 was used to identify the components of the energy model defined in EnergyPlus (Section 2.1.4).

$$0 = Q_{Cooling} + Q_{Envelope} + Q_{Infiltration} + Q_{Equipment} + Q_{Lighting} + Q_{Ventilation} + Q_{Dehumidifier} + Q_{Plants} \quad (1)$$

In Equation 1, $Q_{Cooling}$ is the energy removed from the HPCF through the cooling system, $Q_{Envelope}$ is the heat gained or lost through the HPCF envelope through conduction and radiation, $Q_{Infiltration}$ is the heat gained or lost through air exchange with the outside air through infiltration, $Q_{Equipment}$ is the internal heat

gains due to equipment within the HPCF, $Q_{Lighting}$ is internal heat gains due to electric lighting, $Q_{Ventilation}$ is energy gained or lost through scheduled ventilation, $Q_{Dehumidifier}$ represents the sensible gains and latent losses to the system from the standalone dehumidifier, and Q_{Plants} represents the sensible and latent effects of the plants on the indoor air of the HPCF. Positive values in Equation 1 represent energy gains to the system and negative values represent energy removed from the system. Although occupants were present in the HPCF for a few hours each week, the energy model assumed that occupants and the equipment and lights used exclusively in the presence of occupants did not contribute to the energy balance. The energy balance in Equation 1 is illustrated in Figure 3.

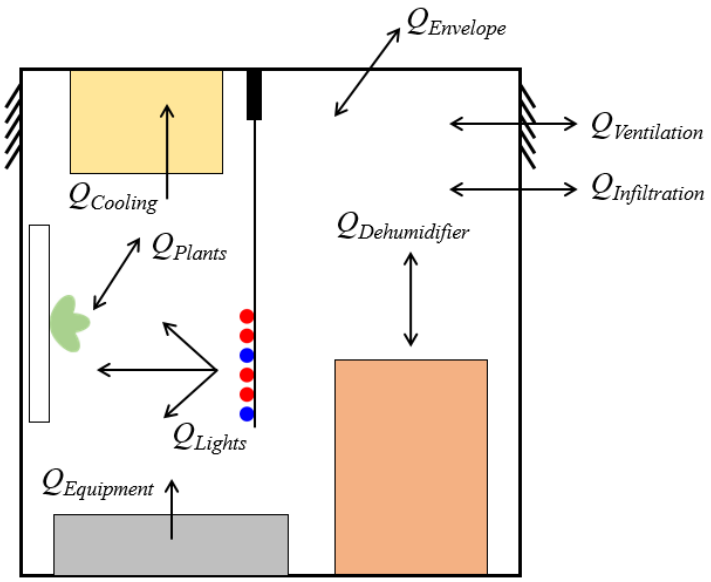

Figure 3: Illustration of terms in Equation 1. Arrows point in the direction of positive energy flow.

Equation 1 is a simplified representation of the container farm assuming steady state operation and no storage of energy or mass. Relevant details, assumptions and interactions associated with each term in Equation 1 are described below. For the purpose of illustrating the theory behind each term in Equation 1, all terms of Equation 1 in this section are given in W. As with the previous work of [14], [26]–[29], this research implemented a parallel model for the latent and sensible effects of plants on the interior air of the container farm. In addition, to better isolate the performance of the energy model in predicting cooling loads, this research also implemented a parallel model based on measured data to incorporate the latent and sensible effects of the dehumidifier within the EnergyPlus model. The methods and assumptions of these two parallel models are also described below.

2.1.2.1 Cooling

In retrofitting the shipping container, Freight Farms installed a Daikin FTK24NMVJU mini-split air conditioner with R410-A refrigerant. The indoor unit was located at the front of the container near the ceiling, and was controlled using a CoolBot temperature controller to maintain an indoor temperature setpoint of approximately 17.5 C. Details regarding the specifications of the cooling system in the EnergyPlus simulation are given in Table 3 in Section 2.1.4.

2.1.2.2 Envelope and Infiltration

In retrofitting the shipping container for use as a hydroponics farm, Freight Farms made minor functional modifications to the exterior structure of the container. However, no modifications were made to the material composition and dimensions of the exterior structure. As such, the values for the interior and exterior dimensions set to standard dimensions, as illustrated in Figure 1. It was assumed that the facades, roof, and floor were constructed of 1.6 mm thick stainless steel with a layer of polyurethane foam as insulation [31]. The farm operator provided the thermal properties of the construction materials and the insulation thickness for the floor, walls, and roof. The exterior of the shipping container, though painted green and white, was assumed to be entirely painted white. Furthermore, it was assumed the infiltration rate for the HPCF was 0.6 ACH. The envelope properties used in defining $Q_{Envelope}$ and $Q_{Infiltration}$ in the energy model are summarized in Table 3 in Section 2.1.4.

2.1.2.3 Equipment

The HPCF operator provided a summary of all equipment within the HPCF, which consisted of the following categories: water and nutrient pumps and regulators; air circulation fans; and miscellaneous components not explicitly necessary for plant growth (such as a video camera). Given the equipment quantities and power ratings, the maximum equipment power load in the HPCF was calculated to be 1247.5 W. The fraction of input energy converted to radiant and convective energy were assumed to be 0.2 and 0.8, respectively, for all equipment. The available equipment power for every hour of the energy model was given by

$$Q_{Equipment} = \eta_{Equipment}(1247.5\ W) \quad (2)$$

where $\eta_{Equipment}$ is the measured hourly load factor of equipment as described in Section 2.1.3.

2.1.2.4 Lighting

The main grow lights in the HPCF consisted of 128 hanging strips of 84 SMD5050 red and blue light emitting diodes (LEDs) [32]. According to the farm operator, the total power rating of the main grow lights was 3840 W. The seedling grow lights, which illuminated two sets of seedling trays with the same SMD5050 red and blue LEDs, had a total power rating of 40 W. Following the methods of [33], the fraction of input electricity to the LED grow lights converted to far-infrared radiation and visible radiation was 0.02 and 0.33, respectively. It was assumed that the remaining fraction of input energy was converted to heat within the HPCF through convection [34].

As described in Section 2.1.2.7, a portion of the visible light energy, R_{Net} in W/ m^2, was intercepted and used by the plants. Consequently, the available lighting power for every hour of the energy model was given by

$$Q_{Lights} = \eta_{Lights}(3880\ W - R_{Net}A_{plants}) \quad (3)$$

where η_{Lights} is the measured hourly load factor of lights as described in Section 2.1.3 and A_{plants} is the total crop surface coverage area in the HPCF in m^2 as described in Section 2.1.2.7. The photoperiod in the HPCF was 18 hours per day.

2.1.2.5 Ventilation

The scheduled ventilation system in the HPCF consisted of one inlet fan located near the front entrance and one exhaust fan located at the rear of the container. Due to the closed nature of plant factories, the ventilation levels of these systems are typically maintained to a minimum to reduce the possibility of outside contaminants entering the farm space. The maximum steady state ventilation rate was estimated by measuring the average air speed exiting the inlet fan at various points (1.98 m/s) and multiplying by the approximate area of the fans (0.018 m^2). The resulting maximum steady state ventilation rate was estimated as 0.035 m^3/s for both the inlet and exhaust fans. For every hour of the energy model, the ventilation rate was specified by

$$\dot{V}_{Ventilation} = \eta_{Ventilation}(0.035\ m^3/s) \quad (4)$$

where $\eta_{Ventilation}$ is the measured hourly load factor of ventilation as described in Section 2.1.3.

2.1.2.6 Dehumidifier

In addition to the mini-split air conditioner, a standalone dehumidifier was installed within the HPCF to maintain indoor relative humidity values between 60-70%. From the specifications of a similar system, the HPCF dehumidifier was assumed to have a rated water removal rate ($\dot{V}_{water,rated}$) of 52 L/day and an energy factor (EF_{rated}) of 3 L/kWh [35]. Additionally, the parasitic loads of the dehumidifier were assumed to be 0 W. The dehumidifier unit, operating fully within the control volume of the HPCF, contributed latent and sensible loads to the indoor air:

$$Q_{Dehumidifier} = Q_{D,Latent} + Q_{D,Sensible} \quad (5)$$

where Q_{D_Latent} and $Q_{D\_Sensible}$ are the latent and sensible loads of the dehumidifier, respectively. The latent and sensible loads of the dehumidifier were calculated following the methods outlined in EnergyPlus "Zone Air DX Dehumidifier" section of the "Engineering Reference" documentation [36] with the exception of substituting the measured hourly load factor for the dehumidifier (η_{dehum}), described in Section 2.1.3, for the part load ratio.

$$Q_{D,Latent} = 1000 \cdot \lambda \cdot \eta_{dehum} \cdot \dot{m}_{water,ss} \quad (6)$$

The latent loads are calculated from Equation 6 where λ is the latent heat of vaporization of water in J/g and $\dot{m}_{water,ss}$ is the steady state dehumidifier water removal rate in kg/s. The steady state dehumidifier water removal rate is calculated by:

$$\dot{m}_{water,ss} = \frac{\rho_w \cdot \dot{V}_{water,rated} \cdot F_w}{24 \cdot 3600 \cdot 1000} \quad (7)$$

where ρ_w is the density of water in kg/m^3, $\dot{V}_{water,rated}$ is the rated dehumidifier water removal rate in L/day, and F_w is the water removal modifier fraction. This fraction is the result of the biquadratic function of indoor temperature (T_{in}) in ˚C and relative humidity (RH_{in}) shown in Equation 8. Similarly, the energy factor modifier fraction, F_P, is calculated using the biquadratic curve in Equation 9. The values for the coefficients in both equations are given in Table 1.

$$F_w = a + b(T_{in}) + c\left(T_{in}{}^2\right) + d(RH_{in}) + e\left(RH_{in}{}^2\right) + f(T_{in} \cdot RH_{in}) \quad (8)$$

$$F_P = a + b(T_{in}) + c\left(T_{in}{}^2\right) + d(RH_{in}) + e\left(RH_{in}{}^2\right) + f(T_{in} \cdot RH_{in}) \quad (9)$$

	F_w	F_p
a	-1.1625	-1.9022
b	0.022715	0.063467
c	-0.00011321	-0.00062284
d	0.021111	0.03954
e	-0.000069303	-0.00012564
f	0.00037884	-0.00017672

Table 1: Generic coefficients of biquadratic performance curves for standalone dehumidifiers [37]

From the steady-state energy balance of the dehumidifier as a system in Equation 10, the sensible loads are equal to the sum of the input electrical power ($P_{D,in}$) and the latent energy of condensing water vapor (Equation 6). $P_{D,in}$ is calculated using Equation 11 where $P_{D,ss}$ is the steady state power consumption of the dehumidifier under given conditions of indoor temperature and relative humidity (Equation 12).

$$Q_{D,Sensible} = P_{D,in} + Q_{D,Latent} \quad (10)$$

$$P_{D,in} = \eta_{dehum} \cdot P_{D,ss} \quad (11)$$

$$P_{D,ss} = \frac{\dot{V}_{water,rated} \cdot F_w \cdot 1000}{EF_{rated} \cdot F_P \cdot 24} \quad (12)$$

Using this process, hourly values for $Q_{D,Latent}$ and $Q_{D,Sensible}$ were calculated in a spreadsheet model for the entire dataset and incorporated in the EnergyPlus model as described in Section 2.1.4.

2.1.2.7 Plants

The parallel model used to incorporate the latent and sensible effects of plant evapotranspiration in the EnergyPlus model was based on satisfying the leaf energy balance of Equation 13. In this energy balance, R_{Net}, is the net photosynthetically active radiation (PAR) absorbed by the leaf surface, Q_{ET} is the latent energy of evapotranspiration released by the leaf, and H is the sensible heat exchange between the leaf surface and the container farm air. All units in Equation 13 are expressed in W/m^2. Due to the relatively small values compared to the energy fluxes at the plant boundary, energy stored in the plant was ignored [25], [26]. Figure 4 illustrates this energy balance at the leaf surface.

$$0 = R_{Net} - Q_{ET} - H \quad (13)$$

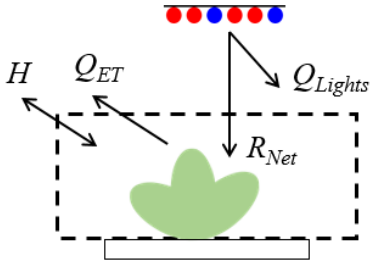

Figure 4: Energy balance at the leaf surface. Arrows point in the direction of positive energy flow.

For every hour of the dataset, values of R_{Net} and Q_{ET} were calculated in a spreadsheet model using the methods described in this section. Values for and H were calculated in the spreadsheet model to satisfy the energy balance of Equation 13. This spreadsheet model was incorporated in the EnergyPlus model as described in Section 2.1.4 where the energy from plants was represented by Equation 14. In this equation, A_{plants} is the total crop surface coverage area in the HPCF in m^2. It was assumed that the HPCF farm, with an approximate vertical cultivation area $A_{cultivation}$ of 42 m^2, was operating at full cultivation capacity of butterhead lettuce for the entire dataset, with 50% of the available cultivation area occupied by the lettuce crops.

$$Q_{Plants} = A_{plants} \cdot (Q_{ET} + H) \quad (14)$$

$$A_{plants} = 0.5 \cdot A_{cultivation} \quad (15)$$

The values for R_{Net} were calculated following the methods used by [25] in Equation 16. In this equation, ρ_r is the reflectivity coefficient of lettuce, R_{PAR} is the PAR reaching the surface of the plant canopy in W/m^2, and *CAC* is the cultivation area cover for lettuce. Following the recommendations of [25], ρ_r and *CAC* are assumed to be 0.07 and 0.9, respectively.

$$R_{Net} = (1 - \rho_r) R_{PAR} CAC \quad (16)$$

The hourly values for R_{PAR} were calculated through Equation 17 where η_{Lights} is the measured hourly load factor for the grow lights (as defined in Section 2.1.3), P_{Lights_max} is the maximum electrical power input of the main grow lights (3840 W), and η_{PAR} is the fraction of the input electric energy of the grow lights converted to PAR. Following the results of [38], η_{PAR} was assumed to be 0.31.

$$R_{PAR} = \frac{\eta_{Lights} \cdot P_{Lights\_max} \cdot \eta_{PAR}}{A_{cultivation}} \quad (17)$$

The hourly latent loads of Q_{ET} were calculated using the Pennman-Monteith equation, Equation 18 [39]. Following the methods of [25], plant transpiration was calculated for a single leaf surface and total crop transpiration was calculated with the addition of a leaf area index (LAI) multiplier to account for the overlapping of leaves within the crop canopy. Measured values for indoor ambient air dry-bulb temperature and relative humidity were used to calculate hourly values for e_s and e_a following the methods in [40].

$$Q_{ET} = \lambda E = LAI \cdot \frac{\Delta(R_{Net} - G) + \rho_a c_p(\frac{e_s - e_a}{r_a})}{\Delta + \gamma(1 + \frac{r_s}{r_a})} \quad (18)$$

where:

λ is the latent heat of vaporization of water in J/g
E in the water evapotranspiration rate in g/s-m^2
LAI is the leaf area index
Δ is the slope of the vapor pressure curve in Pa/C
R_{Net} is the net radiation falling on the surface of the plant canopy in W/m^2
G is the ground heat flux, assumed to be 0 W/m^2
ρ_a is the density of air in kg/m^3
c_p is the specific heat capacity of air in J/kg-K
e_s is the saturation vapor pressure of the ambient air in Pa
e_a is the vapor pressure of the ambient air in Pa
γ is the psychrometric constant in Pa/C
r_s is the stomatal resistance to vapor transfer in s/m
r_a is the aerodynamic resistance to vapor transfer in s/m

As reviewed by [41], there exist many methods with varying degrees of simplification to estimate the crop-specific variables of Equation 18: r_s, r_a, and LAI. Following previous work, this research used two simplified methods to determine the values of these crop-specific variables. Because the indoor air velocity in the HPCF was unknown, the crop aerodynamic resistance r_a, which is primarily driven by airflow, was assumed to be a constant 100 s/m for an indoor environment with forced air circulation as done by [25]. The stomatal resistance r_s for lettuce was also determined using the methods of [25] following the hypothesis that r_s is primarily influenced by light intensity, which is also discussed by [41]. The work of [25] estimated this relationship in Equation 19 by extrapolating from measured data of stomatal conductance in response to varying irradiance levels.

$$r_s = 60 \cdot \frac{1500 + PPFD}{200 + PPFD} \quad (19)$$

In Equation 19, PPFD is the photosynthetic photon flux density in μmol/m^2/s. For the HPCF, the PPFD available to the plants in the main grow area was estimated to be 100-130 μmol/m^2/s [32]. However, throughout the dataset, PPFD levels varied with varying lighting levels. To better estimate values of r_s, PPFD was calculated using Equation 20 where η_{Lamp} is the efficacy of the LED lights in photons per joule in PAR emitted by the lamp. The value for η_{Lamp} was 5.2 μmol(PAR)/J(PAR) following the methods of [38]. The calculated values of r_s using Equation 19 were verified against measured r_s data for lettuce under comparable lighting conditions [42].

$$PPFD = R_{Net}\eta_{Lamp} \quad (20)$$

Finally, following the work of [25], a constant LAI value of 2.1 was used to represent a uniform distribution of lettuce at different growth stages. The calculated hourly values for *E* were verified against evapotranspiration values under comparable lighting conditions from the simulations of [25].

2.1.3 Data Collection and Processing

For the purposes of creating the energy model and validating its performance, two sets of data were collected. The first dataset collected interior HPCF climate data, exterior site climate data, and HPCF energy consumption data from August 2018 until August 2019. The second dataset was provided by the HPCF operator and contained lighting and equipment use logs during the same time period. This Section describes the methods used to collect each of these datasets and how these data were used to define and validate the energy model.

Climate and Energy Data

An Onset Computer Corporation HOBO U30 Wi-Fi Data Logger was used to collect climate and energy data. This data logger was stationed on the roof of the HPCF and collected outdoor climate data, indoor climate data, and energy usage data for the entire HPCF as well as individually for the heat pump. The same type of data logger was used to collect solar radiation and ambient air pressure data from the roof of a five story building (referred to as “Building 1”) located 10 miles north of the HPCF site.

The data logger was set to collect data every minute from the sensors in Table 2. The measurements in the two sets of climate data shown in Table 2 were averaged to obtain hourly values for use as direct and indirect inputs in the energy model. The measurements for energy data listed in Table 2 were aggregated to obtain total hourly values for use in the energy model validation.

	Data Collected	Sensor	Location
Outdoor Climate	Outdoor Air DP, RH, DB T	S-THB 10290123:10268926	Roof of HPCF
	Wind Direction	S-WDA 10290123:10260437-1	
	Wind Speed	S-WSB 10290123:20425730-1	
	Solar Radiation	S-LIB 10290124:2375831-1	Roof of Building 1
	Pressure	S-BPB 10290124:10236707-1	
Indoor Climate Values and Control	Inlet and Exhaust Ventilation Fans	S-FS-TRMSA 10290123:20431081-1	electrical box
	Return Air DP, RH, DB T	S-THB 10290123:20420500	Heat pump RA
	Supply Air DB T	S-TMB 10290123:20435677-1	Heat pump SA
	Heat Pump Fan Current	S-FS-TRMSA 10290123:20431082-1	electrical box
Energy Usage	Main Power	S-UCC 10290123:20441881-1	electrical box
	HP Power	S-UCC 10290123:20441882-1	electrical box

Table 2: Climate and Energy Data collected from the roof of the HPCF and, for Solar Radiation and Ambient Pressure, from the roof of a 5-story building located 3 miles northeast of the HPCF

Lighting and Equipment Schedule and Load Data

The HPCF operator provided usage logs that reported, for every minute of the dataset, whether all components were "on" or "off" in the categories of lighting, equipment, ventilation, and dehumidifier. These values were first converted into binary usage data and then averaged to obtain hourly percentage usage values η_c for each component *c*.

Using the nominal power consumption and calculated η_c for all components in each category, a fraction value from 0 to 1 was calculated to represent the "measured hourly load factor" during that hour for the lighting (η_{Lights}), ventilation ($\eta_{Ventilation}$), equipment ($\eta_{Equipment}$), and dehumidifier (η_{dehum}). Equation 21 shows this process to calculate η_{Lights} as an example.

$$\eta_{Lights} = \frac{\sum_c \eta_c P_{Nominal,c}}{\sum_c P_{Nominal,c}} \quad (21)$$

2.1.4 Defining the Energy Model

The energy model for this study predicted the $Q_{cooling}$ loads of the HPCF in Equation 1. The container farm was modeled as a single thermal zone building in the architectural 3D modeling program Rhinoceros 6.0™ [43] and the EnergyPlus simulation engine, version 8.4.

Three main categories of inputs were specified in the energy model to reflect Equation 1 in Section 2.1.2: internal loads; interior conditioning setpoints and operation; and envelope construction. These main inputs are summarized in Table 3. The values required for these inputs were obtained through a combination of the measured data, given load and schedule information, and assumptions discussed in Section 2.1.2.

Category	Input	Units	Source	Value
Internal Loads	Lighting Power Density	W/m^2	HPCF Operator	130
	Lighting Fraction Radiant	0-1	[33]	0.02
	Lighting Fraction Visible	0-1	[33]	0.33
	Equipment Power Density	W/m^2	HPCF Operator	51
	Equipment Fraction Radiant	0-1	Assumption	0.2
	Dehumidifier Latent Losses Power Density	W/m^2	Section 2.2.1	-62
	Dehumidifier Sensible Gains Power Density	W/m^2	Section 2.2.1	92
	Dehumidifier Fraction Raciant	0-1	Assumption	0.2
	Plants Latent Gains Power Density	W/m^2	Section 2.2.1	72
	Plants Sensible Losses Power Density	W/m^2	Section 2.2.1	-53
Conditioning Setoints and Operation	Ventilation Rate	m^3/s	Measured	0.035
	Cooling Setpoint	C	HPCF Operator	17.5
	Max. Relative Humidity Setpoint	%	Measured interior climate data	70
	Min. Relative Humidity Setpoint	%	Measured interior climate data	60
Envelope Construction	Floor U-Value	W/m^2-K	HPCF Operator	0.18
	Walls and Roof U-Value	W/m^2-K	HPCF Operator	0.43
	Façade Exterior Surface	-	HPCF Operator	White Paint
	Façade Interior Surface	-	HPCF Operator	Stainless Steel
	Infiltration	ACH	Assumption	0.6

Table 3: Energy model principal inputs and values for the template container farm[1]

As described in Section 2.1.2, the parallel models used in this study were two spreadsheet models that, for every hour of the dataset, calculated latent and sensible loads in W for the plants and dehumidifier. These parallel models were incorporated in the EnergyPlus model by creating four custom objects under the category “Other Equipment” (a sensible and latent object each for the plants and the dehumidifier). The

[1] A complete EnergyPlus input data file for the template container farm is given in the supplementary material of this thesis.

power densities for these objects were defined as the extreme values for each load type (sensible and latent) across the entire dataset. These inputs are shown in in Table 3 along with values specified for the container farm template (Section 2.2.1).

The schedules for the custom objects of the plants and dehumidifier were defined as schedule arrays of values between 0 and 1 to represent the calculated fraction of the maximum or minimum loads occurring at each hour. Similarly, schedule arrays of the measured hourly load factors (Section 2.1.3) were used for the lights, equipment, and ventilation objects.

The weather file used for the energy model was based on the Boston-Logan Intl AP 725090 Typical Meteorological Year 3 (TMY3) EnergyPlus Weather File (EPW). The weather files was edited to include the measured outdoor climate data listed in Table 2.

The energy simulation was run for a year at an hourly resolution with a timestep of 10 minutes. The outputs of the EnergyPlus simulation were ideal total cooling loads, equipment energy use, and lighting energy use. To obtain the predicted cooling energy, the output of the simulation was divided by the coefficient of performance (COP) of the heat pump; this is described in further detail in Section 2.1.4.

2.1.5 Energy Model Post-Processing: COP Sub-Models

Following the simulation of the HPCF in EnergyPlus, the application of a COP was required to obtain hourly predictions for the mini-split heat pump energy consumption, E_{HP_Sim}. For every hour *i* of the dataset, the raw output ideal cooling loads from EnergyPlus, $Q_{Cooling,i}$, were divided by hourly COP values, COP_i, to obtain the predicted hourly heat pump energy consumption, $E_{HP\_Sim,i}$ (Equation 22).

$$E_{HP\_Sim,i} = \frac{Q_{Cooling,i}}{COP_i} \quad (22)$$

Three different sub-models were used to obtain hourly COP values. The first sub-model, referred to as the "measured COP", calculated COP values from measured heat pump energy and psychrometric data. This model was used for an initial validation of the assumptions made in for the various components of Equation 1.While the measured COP model enabled this initial validation, this is not a practical option for general energy models of plant factories. Therefore, the next two COP sub-models represented options available to designers predicting future energy use of plant factories. The second COP sub-model,

referred to as "constant COP," assumed a constant COP obtained from the average COP provided in manufacturer specifications of the heat pump. The third COP sub-model, referred to as "COP equation," calculated COP values as a function of outdoor air temperature. Details and assumptions regarding each of these COP sub-models are provided below.

Measured COP

The first method calculated the average measured COP of the heat pump, $COP_{measured,i}$, for every hour *i* in the study. This was done by calculating $COP_{measured,k}$ for every time step *k* of data collection (Section 2.1.3) and finding the average COP for each hour of the dataset. The calculation for $COP_{measured,k}$ is given by Equation 24 where *t* is the data collection time step in seconds, $q_{removed,k}$ is the energy removed from the air passing through the heat pump in kW for every time step of data collection, and $q_{in,k}$ is the measured energy consumed by the heat pump in kJ. Equation 24 gives the calculation for $q_{removed,k}$ where ρ_{air} is the density of air in kg/m^3, $\dot{V}_{air}$ is the volumetric flow rate of the indoor air flowing through the heat pump in m^3/s, and h_{SA} and h_{RA} are the specific enthalpies in kJ/kg of the heat pump supply air and return air respectively. $q_{Condensate,k}$ is the calculated energy removed via the condensate in kW and is given by Equation 25 where $h_{condensate}$ is the enthalpy of liquid water at the supply air temperature and w_{SA} and w_{RA} are the humidity ratios in g/kg$_{d.a.}$ of the heat pump supply air and return air respectively.

$$COP_{measured,k} = \frac{t \cdot (q_{removed,k} + q_{removed,k-1})/2}{q_{in,k}} \quad (23)$$

$$q_{removed,k} = \rho_{air}\dot{V}_{air}(h_{SA} - h_{RA}) - q_{Condensate,k} \quad (24)$$

$$q_{Condensate,k} = \frac{\rho_{air}\dot{V}_{air}h_{condensate}(w_{SA} - w_{RA})}{1000} \quad (25)$$

The volumetric flow rate $\dot{V}_{air}$was estimated using a function of the measured current of the heat pump's fan. This equation was derived by conducting a hooded balometer test to relate measured volumetric flow rate to measured fan current (Equation 26). The R^2 for Equation 26 was 0.9984.

$$\dot{V}_{air} = 2185.6\ ({I_{fan}}^{0.4162}) \quad (26)$$

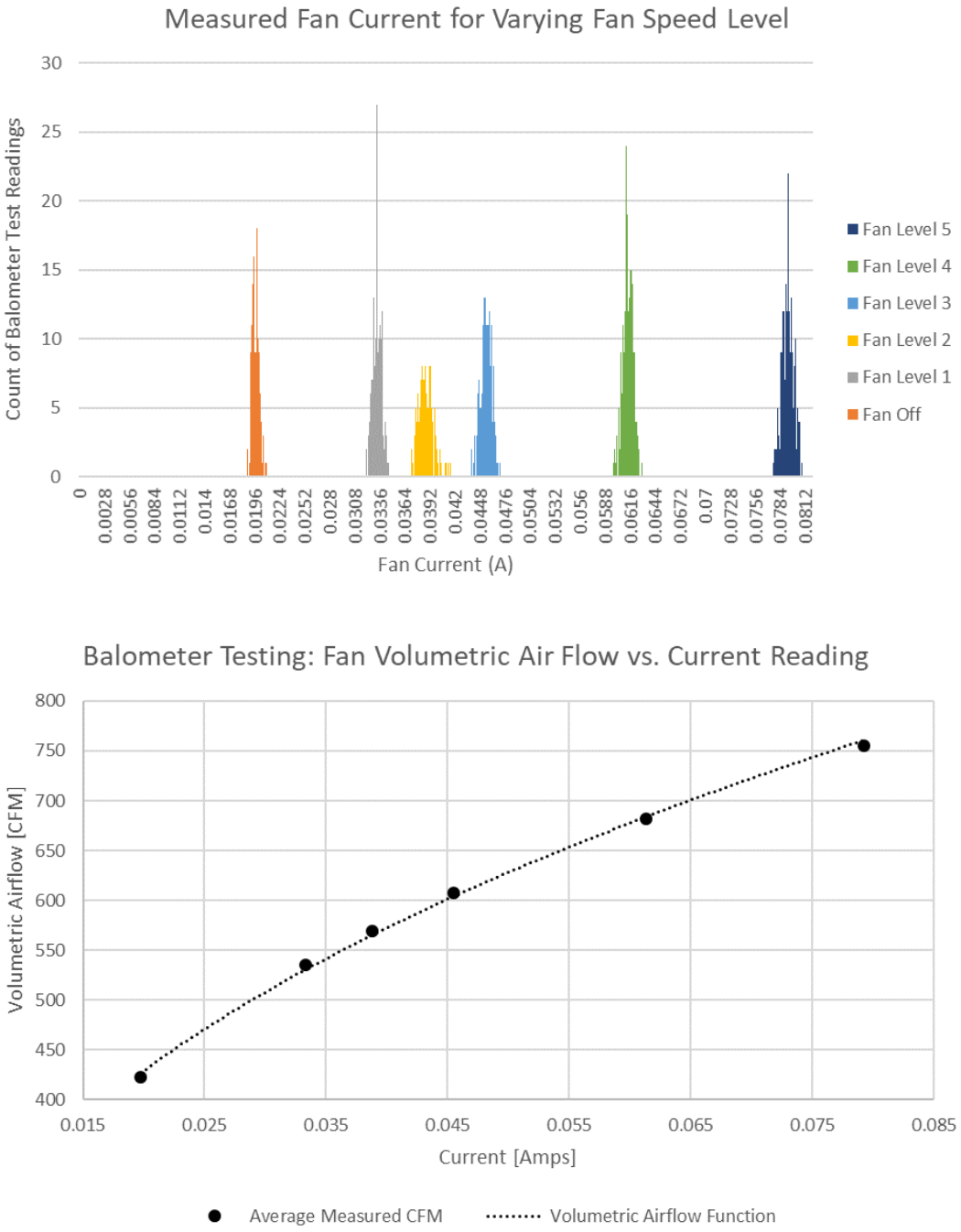

Figure 5: Balometer test results (top) and the derived volumetric flow rate of fan air as a function of fan current (bottom)

The enthalpies and humidity ratios of the supply and return air were estimated using the methods outlined in the 2017 ASHRAE Handbook: Fundamentals [40]. For these calculations, it was assumed that the relative humidity of the supply air remained constant at 98%, unless the return air was sufficiently dry

that dehumidification could not occur. In the latter case, the humidity ratio was held constant to that of the return air.

A valid $COP_{measured}$ value was calculated using Equation 24 only if the following two conditions were met. The first condition was for the measured fan current of the heat pump, I_{fan}, to exceed a threshold of 0.028 A. The second condition was that the measured power consumption of the heat pump, $\dot{q}_{in}$, exceed the minimum power rating of 0.29 kW. Values for $COP_{measured}$ were calculated for every minute of the dataset and all valid values were averaged to obtain a single hourly $COP_{measured}$ value. If no valid $COP_{measured}$ values were calculated for all minutes in a given hour of the dataset, the hourly $COP_{measured}$ was flagged as invalid. Finally, to avoid artificially low COP values due to the averaging process, the final hourly $COP_{measured}$ values were capped at a minimum of 3 (the manufacture rated minimum was 3.66).

Constant COP

For the heat pump installed in the HPCF, the manufacturer documentation provided an average, rated maximum, and rated minimum COP value. Because the HPCF was located in a climate with both hot and cold temperatures throughout the year, the manufacturer-specified seasonal energy efficiency ratio (SEER) COP of 5.27 W/W was used as the constant COP, $COP_{constant}$. However, if this method were to be implemented for container farms or plant factories located in climates with predominantly extreme hot or cold temperatures, rated minimum and rated maximum COP values may be used as constant COP value, respectively.

COP Equation

The COP equation sub-model used manufacturer specifications to approximate COP as a function of outdoor air temperature, T_{out} in ˚C (Daikin Industries, Ltd.). This equation (Equation 27) was derived from the manufacturer's capacity tables relating indoor air dry bulb temperature, indoor wet bulb temperature, outdoor air temperature, total heat pump capacity, and power input. The indoor air dry bulb temperature and relative humidity setpoints in the HPCF were 17.5˚C and 60-70%, respectively. However, in the capacity tables the minimum indoor air dry bulb temperature was 20˚C and the relative humidity was calculated as a constant value of 50%. Consequently, rated COP values, COP_{tables}, were approximated assuming a constant indoor air temperature of 20˚C using Equation 27.

$$COP_{tables} = \frac{total\ capacity}{power\ input} \quad (27)$$

Given the calculated values of COP_{tables} for outdoor air temperatures between 20˚C and 40˚C and an additional manufacturer-specified COP value for the same interior conditions at an outdoor dry-bulb air temperature of -15˚C, the trendline functionality in Microsoft Excel was used to approximate an equation for heat pump COP (Equation 28). This was then bounded by the rated minimum COP value and the rated COP values at -15˚C to obtain the final COP equation sub-model, $COP_{equation}$ (Equation 29).

$$f(T_{out}) = -0.143 \cdot (T_{out}) + 8.1604 \quad (28)$$

$$COP_{equation} = \begin{cases} COP_{equation} \leq COP_{Rated_{Min}}, COP_{Rated_{Min}} \\ all\ else, f(T_{out}) \\ COP_{equation} \geq COP_{-15^{\circ}\mathrm{C}}, COP_{-15^{\circ}\mathrm{C}} \end{cases} \quad (29)$$

2.1.6 Model Validation

For every hour *i* in the dataset, the HPCF energy model was validated against measured energy values for both total energy, $E_{Total_{Measured},i}$, and cooling energy consumption of the heat pump, $E_{HP_{Measured},i}$. Several filters were applied to the dataset prior to comparing measured and simulated results to remove hours during which data were missing or invalid. Only hours during which all data categories in Section 2.1.3 contained values were considered in the validation analysis. Additionally, only hours with valid COP values for $COP_{measured}$, as described in Section 2.1.5, were considered in the analysis. Finally, only hours for which the average lighting levels for 12 hours before and 11 hours after (totaling a 24 hours period centered on the hour in question) exceeded a value of 50% were used in the validation analysis. This excluded periods of time in the dataset with significantly low lighting levels but retained the 6 daily hours during which the lights were off (for example, if the farm was operating at only 25% capacity).

2.2 Upgrade and Climate Scenarios Methods

Upon validating the energy model for the HPCF, an energy model for a generic template container farm was created based on the HPCF. This section describes the methods of creating the template container farm energy model and simulating various upgrade scenarios to the template container farm for cities in varying climates.

2.2.1 Creation of a Template Energy Model of a Shipping Container Farm

The purpose of defining the template container farm energy model was to characterize the HPCF under normal operating conditions to produce a generic energy model that could be used by designers in future analyses of container farms. Normal operating conditions were defined by periods of consistent lighting schedules when the HPCF was operating at full capacity (i.e., where η_{Lights} was on a 12-hour cycle with 9 hours with a value above 0.9 followed by 3 hours with a value below 0.1). The energy model inputs for the template container farm were the same as those used for the HPCF energy model listed in Table 3. Additionally, the $COP_{equation}$ described in Section 2.1.5 was used to model the COP as a function of outdoor air dry-bulb temperature. This section describes the process used to define normal operating schedules for the template container farm for lighting, equipment, and ventilation. Additionally, this section describes the process to calculate the hourly schedules for the dehumidifier and plants during normal operation and the associated sensible and latent loads. As with the validation energy model, all generic hourly schedules were defined using hourly load factor values between 0 and 1 and were assumed to repeat daily.

Generic Lighting Schedule

The HPCF operator specified the normal lighting schedule as 12-hour cycles with a photoperiod of 9 hours where all grow lights were on followed by 3 hours where all grow lights were off. This section refers to these two light periods as the "lights on" and "lights off" periods, respectively. This pattern was verified from the measured lighting schedule data provided by the HPCF operator. All subsequent schedules were specified as hourly load factors between 0 and 1 during "lights on" and "lights off" periods.

Generic Equipment Schedule

Figure 6 shows the hourly equipment hourly load factors during regular "on" and "off" light periods. While there was significant spread during both lighting periods, the mean hourly equipment hourly load factors were calculated as 0.5 for "lights on" and "lights off" periods.

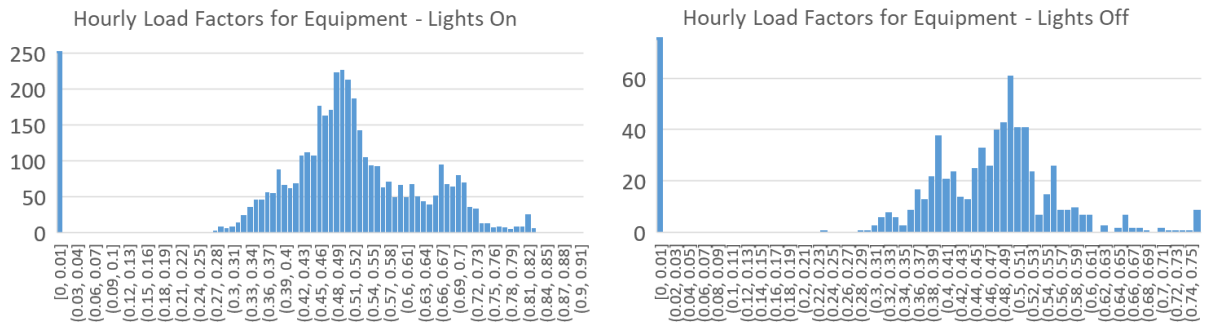

Figure 6: Measured equipment hourly load factors during regular "lights on" (left) and "lights off" (right) periods

Generic Ventilation Schedule

To determine a generic ventilation schedule, it was first calculated that 15% of ventilation hours occurred during "lights on" periods and 85% of ventilation hours occurred during "lights off" periods. Additionally, because ventilation occurred during only 2% of hours during the lights "on" period, it was assumed that the generic ventilation schedule was limited to lights "off" hours. Finally, it was calculated that, during total regular operation hours for the dataset, ventilation occurred during 13% of those hours, which corresponds to approximately 3 hours a day of ventilation for the generic ventilation schedule. The graphs in Figure 7 were used to determine a constant ventilation hourly load factor for the generic schedule. From Figure 7 a), it was determined that 89% of hourly ventilation hourly load factors were between 0.007 and 0.05 (excluding values of 0.0). Therefore, the graph from Figure 7 b) examined hourly ventilation hourly load factors between 0.007 and 0.05. Of the hourly ventilation hourly load factors within this range, 68% were in the cluster between 0.015 and 0.02 (Figure 7 (b)). The average of the hourly load factors in this range, 0.0175, was rounded up to 0.02 as the final, constant ventilation hourly load factor for the template container farm.

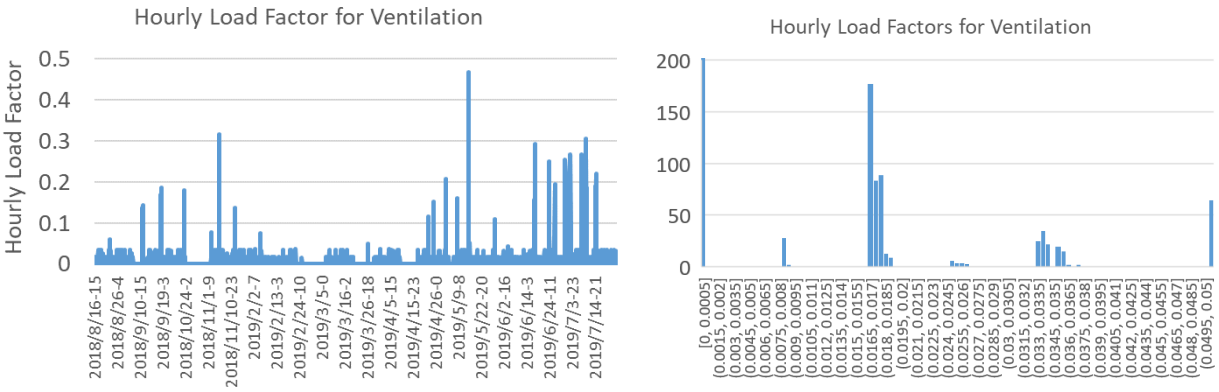

Figure 7: Ventilation hourly load factors during all hours of regular HPCF operation as a time series (left) and histogram (right)

Generic Dehumidifier Schedule and Loads

Figure 8 shows the dehumidifier measured hourly load factors during regular "on" and "off" light periods. Despite significant variations in the dehumidifier measured hourly load factors during the "lights on" period, the load factor for the generic dehumidifier schedule during "lights on" periods was assigned the mean value of 0.5. The load factor for the "lights off" periods was assigned the mean value of the measured hourly load factor during "lights off" periods, 0.8.

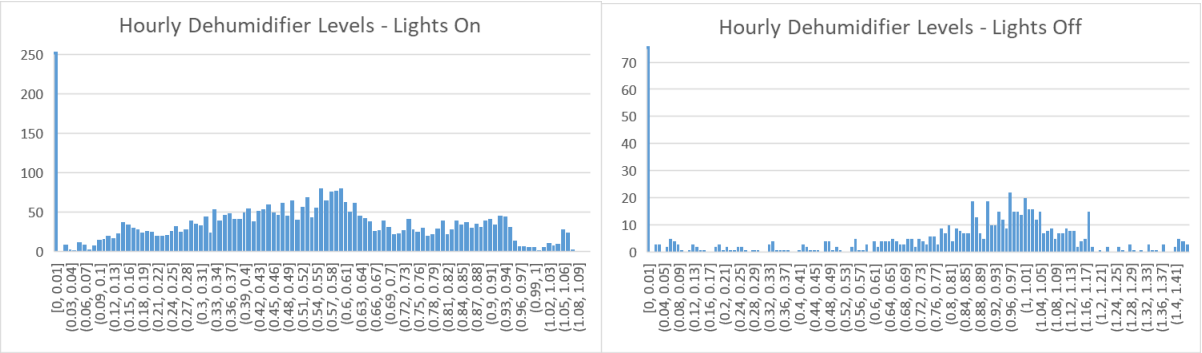

Figure 8: Measured dehumidifier hourly load factors during regular "lights on" (left) and "lights off" (right) periods

Given the dehumidifier hourly load factors for the regular operation of the template container farm, the sensible and latent loads of the dehumidifier were calculated using a modification of the methods described in Section 2.1.1. Whereas Equation 6 and Equation 10 calculated latent and sensible loads in part as a function of indoor temperature and relative humidity, that was not possible for the template container farm. Instead, a linear relationship was found between the calculated rate of water removal (from Section 2.1.1) and the measured hourly load factor for the dehumidifier (Figure 9). This linear relationship is expressed in Equation 30 where $\dot{m}_{water,G}$ is the rate of water removal in kg/h for the dehumidifier in the template container farm.

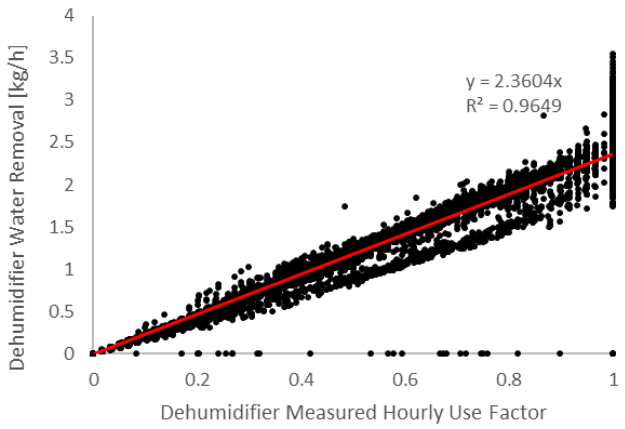

Figure 9: Relationship between the dehumidifier measured hourly load factor and calculated water removal rate.

$$\dot{m}_{water,G} = 2.3604\ (\eta_{dehum}) \tag{30}$$

With this expression, the template container farm dehumidifier latent load, $Q_{D_{Latent},G}$, was calculated in W using Equation 31.

$$Q_{D_{Latent},G} = \frac{1000 \cdot \lambda \cdot \dot{m}_{water,G}}{3600} \tag{31}$$

The template container farm dehumidifier sensible load, $Q_{D_{Sensible},G}$, was calculated using Equation 32, similarly to Equation 10. However, whereas in Equation 10 the expression for the power consumption of the dehumidifier was in part a function of indoor temperature and relative humidity, Equation 3332 expresses the template container farm dehumidifier power consumption, $P_{D,in,G}$, in W as a function of $\dot{m}_{water,G}$ and the rated energy factor, EF_{rated} (L/kWh).

$$Q_{D_{Sensible},G} = Q_{D_{Latent},G} + P_{D,in,G} \tag{32}$$

$$P_{D,in,G} = \frac{1000 \cdot \dot{m}_{water,G}}{\rho_w \cdot EF_{rated}} \tag{33}$$

The extreme values of latent and sensible loads of the template container farm dehumidifier were then calculated using a value of 1 for η_{dehum}. These values are listed in Table 3.

Generic Plant Schedule and Loads

The schedules for latent and sensible loads due to plants in the template container farm were assumed to directly follow the lighting schedule. The values for latent and sensible loads of the plants were calculated using the methods in Section 2.1.1 assuming a constant interior environment of 17.5˚C and 65% RH, a η_{Lights} value of 1 during the "lights on" period and a η_{Lights} value of 0 when during the "lights off" period. The extreme values of latent and sensible loads of the template container farm plants are listed in Table 3.

2.2.2 Modelling System Upgrade Scenarios in Varying Climates

Much like a designer would explore the effects of operating a container farm in varying climates or while implementing energy-reduction strategies, this section describes how the template container farm energy model was used to quantify the effects on annual and peak cooling loads of various upgrade scenarios in cities with varying climates. Five cities in different ASHRAE climate regions were used for this study: New Orleans (2A, hot and humid), Phoenix (2B, hot and dry), Boston (6A, cold and humid), Denver (6B, cold and dry), and Anchorage (7, very cold). For each city, the Typical Meteorological Year 3 weather file was used to run an hourly annual energy model in EnergyPlus (version 8.4) for a baseline scenario (no upgrades) and for each of three upgrade scenarios: addition of insulation, addition of exterior shading, and shifting the lighting schedule. Additionally, a fifth scenario was simulated for each city with combined upgrades of shifting the lighting schedule and adding insulation. The three types of upgrades are described below.

Insulation

While the HPCF was built out of a retired refrigerated shipping container and already contained insulation in the roof, walls, and floor, it was of interest to simulate the effects of increasing insulation to the container's envelope. Many energy efficiency initiatives promote the addition of insulation to building envelopes as a given means to reduce annual building energy demands. However, while these strategies may reduce the energy demands of space conditioning in residential and commercial buildings, the benefit of reducing the heat transfer between the interior of cooling-intensive plant factories and the outdoor environment is not straightforward. Given the large internal sensible heat gains in plant factories from lighting and equipment, it seems plausible that even in hot climates where heat gains through the

building envelope may be significant, addition of insulation may increase overall cooling loads by resisting heat loss through the envelope during hours where the exterior temperature is cooler than the interior temperature. Furthermore, in cold climates where the exterior of the plant factory is significantly colder than the interior environment, it may be beneficial to reduce the insulation and promote heat rejection through conduction. To explore these questions, upgrades to the envelope were made to decrease the U-value of the roof and walls to match that of the floor, 0.18 W/m^2-K.

External Shading

The addition of an opaque, white material was added 1m above the roof of the template container farm and 1m offset from the south, east, and west facades to explore the addition of shading as a strategy for reducing peak and annual cooling loads. In an urban context, such shading may come from a neighboring structure or strategic placement of sun barriers.

Lighting Schedule Shift

As seen in the results presented in Section 3.1, lighting loads account for more than half of the annual energy loads in container farms and are responsible for a large portion of the internal sensible heat gains. One strategy that designers may simulate would be shifting the photoperiod schedule such that the grow lights are not in use during the hottest hours of the day. This strategy is already promoted by utility companies for reducing the energy costs of plant factories during periods of high grid demand. To explore the effects of this strategy, an upgraded light schedule was defined where, rather than having two 12-hour lighting cycles per day, each day contained one 18-hour photoperiod with a 6-hour "lights off" period beginning at 12:00PM. The equipment, ventilation, dehumidifier, and plant schedules were shifted in accordance to the new lighting schedule.

2.3 Grid Integration Methods

This section describes the methods used in a hypothetical case study of a large-scale implementation of container farms in an urban neighborhood in Boston, MA. The purpose of the case study was to explore the effects on the energy demand of the neighborhood with the addition of sufficient container farms to meet the annual vegetable demands of the neighborhood's residents. Section 2.3.1 describes the neighborhood used in this case study and the methods used to calculate the required number of shipping

container farms. Section 2.3.2 describes the methods used in the case study to reduce the additional peak energy demand during the hottest day of the year due to the introduction of container farms.

2.3.1 Neighborhood Description and Calculation of Vegetable Demand

The neighborhood used in this case study was a hypothetical mixed-use neighborhood in Boston, MA consisting of residential, office, and commercial spaces. Thes neighborhood had been proposed as a typical mixed-use neighborhood by students at the Massachusetts Institute of Technology for a graduate course "*4.433 Modeling Urban Energy Flows*" in the spring of 2017. The neighborhood was modeled in umi, an urban building modeling plugin tool for Rhinocerous3D [45]. The building properties and use schedules were defined using buildings templates previously developed by [46] for archetypical buildings in Boston, MA. To obtain hourly neighborhood energy loads, the umi Energy module was used to run an EnergyPlus hourly annual building energy simulation for the neighborhood [45]. The Boston TMY3 weather file was used for the energy simulation.

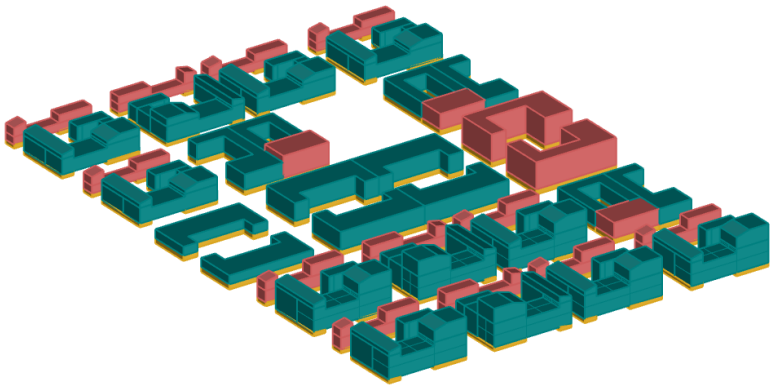

Figure 10: Screenshot of the mixed-use neighborhood in Boston, MA (green, red, and yellow are residential, office, and commercial spaces, respectively).

In addition to using the Energy module to obtain hourly energy loads for the neighborhood, the umi Harvest module was used to estimate the number of template container farms necessary to meet the annual vegetable demands of the 5,153 residents of the neighborhood [22]. For an annual vegetable demand rate of 0.076 tons/person/year, the Harvest module predicted that the neighborhood would require 780 template container farm s, which together would occupy an area equivalent to 42% of the building footprint area in the neighborhood.

2.3.2 Load Reduction

With the addition of the 780 template container farms to the neighborhood, it was of interest to quantify the increase in hourly energy demands of the neighborhood. Due to the cooling-intensive energy demands of container farms, the hottest day of the year for the Boston TMY3 weather file, July 7, was considered for the analysis.

Three scenarios were considered for the addition of the 780 template container farms to the neighborhood. The first scenario considered staggered lighting schedules among the 780 template container farms where each template container farm could have one of 24 lighting schedules that varied in the hour during which the 6-hour "lights off" period occurred. As with the methods used in Section 2.2.2, the equipment, ventilation, dehumidifer, and plant schedules followed all modifications to the lighting schedules. The objective in this first scenario was to minimize the increase in peak energy demand for July 7 while maintianing an 18-hour photoperiod for all 780 template container farms. The second scenario considered turning off the lights for all 780 template container farms throughtout the entire day. The objective in this second scenario was to quantify the minimum amount of additional energy required in the neighborhood in the event that a day's worth of plant growth was sacrificed for the sake of reducing added demands on the grid. The photoperiod for the second scenario was zero hours. The third scenario sought to explore an example of increasing photoperiod hours while not exceeding the minimum additional energy from the second scenario. All container farms were set to operate on the same schedule for the third scenario.

EnergyPlus was used to run hourly energy simulations for a single template container farm using the Boston TMY3 weather files for July 7 using the various lighting schedules. The first scenario required 24 separate energy simulations, shifting the template container farm lighting schedule by an hour with each simulation. Additionally, a baseline scenario was run to obtain the hourly energy demand of the neighborhood without the addition of template container farms.

A spreadsheet model was created in Microsoft Excel to combine the baseline hourly energy demands of the neighborhood with the hourly energy demands of the 780 template container farms. For the first scenario, a manual process was used to scale the energy model results of each of the 24 versions of the template container farm in such a combination that reduced the increase in total neighborhood peak energy demand from the addition of 780 template container farms. For the second and third scenarios, the energy simulation results of the single shipping container were scaled up to approximate the energy demands of all 780 template container farms.

3 Results

3.1 Energy Model Validation Results

Overall, the average daily measured energy consumption of the HPCF was 116.9 kWh/day, just under the 120 kWh/day claimed by the manufacturer. Of this average daily measured value, 16% of the total energy consumption was due to cooling loads (Figure 11). The validation results of this research are presented in two parts: validation of the physics-based energy model and validation of the COP sub-models applied to the energy model results. These results are summarized in Table 4. It is important to note that as seen in Figure 11, the energy model consistently overestimates the lighting, equipment, and dehumidifier loads.

		Hourly Whole Building		Hourly Cooling		Daily Cooling	
	Model Scenario	NMBE (%)	CV(RMSE) (%)	NMBE (%)	CV(RMSE) (%)	CV(RMSE) (%)	
Physics Validation	No Plants (COP Measured)	3	9	-19	36	22	
	With Plants (COP Measured)	3	9	-15	36	19	"Validation"
COP Model Validation	With Plants (COP = 5.27)	6	13	1	50	32	"Simplified"
	With Plants (COP Equation)	4	10	-12	42	22	"Recommended"

Table 4: Summary of energy model validation results

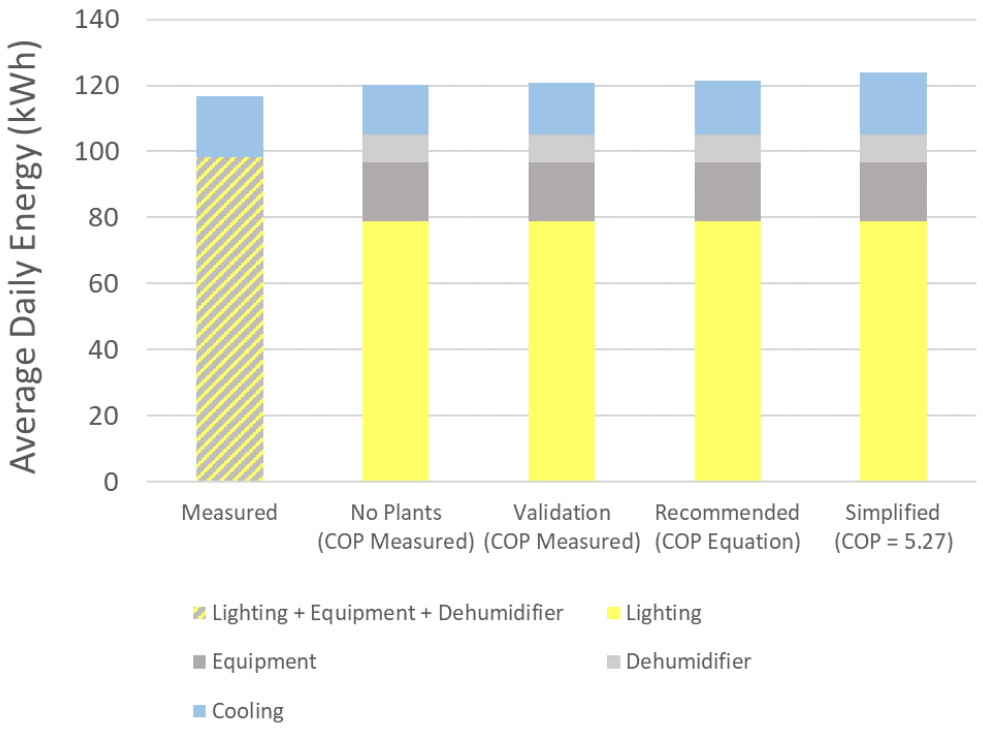

Figure 11: Average daily energy consumption of the HPCF for measured data and energy simulation results.

The first validation quantifies the reliability of the physics-based EnergyPlus model in predicting hourly and daily cooling loads when incorporating the parallel models for sensible and latent effects of plants on the building interior environment. This first validation applied measured COP values to better isolate the effects of plants on the energy model and showed that over the entire dataset, incorporating the latent and sensible effects of plants in the energy model versus omitting the plants reduced the Normalized Mean Bias Error (NMBE) of hourly and daily cooling loads from -19% to -15%. Such an improvement in the model's reliability was not seen in the whole building energy model, where the NMBE values remained the same. While the hourly whole building and hourly cooling Coefficient of Variation of the Root-Mean-Square Error (CV[RMSE]) values are equal between the two scenarios in the initial validation, the daily CV(RMSE) value is lower for the scenario with plants in the energy model, indicating a better performance at the daily timescale for predicting cooling loads. Finally, both scenarios are in meet hourly whole building calibration criteria as specified by [30] (less than 10% NMBE and less than 30% CV[RMSE]).

It should be noted that as an effect of simulating the plant evapotranspiration and the water removal of the dehumidifier in parallel models, the EnergyPlus simulation did not accurately account for a mass balance of the water vapor in the HPCF. Consequently, the EnergyPlus simulation predicted indoor air relative humidity values consistently lower than measured values and predicted indoor values of less than 5% relative humidity during approximately 25% of the simulation hours. As a post-processing analysis, a mass balance of water vapor in the HPCF air was calculated for every hour in the dataset using Equation 34 to explore discrepancies in the mass balance of the parallel models. In the equation, $m_{w,plants}$ is the calculated water contributed through the evapotranspiration of plants without the LAI multiplier, $m_{w.outdoor\ air}$ are the EnergyPlus simulation results of net water added or removed due to infiltration and ventilation, and $m_{w,AC\ condensate}$ and $m_{w,D\ condensate}$ represent the calculated water removed from the zone air from the mini-split air conditioner and dehumidifier, respectively (Section 2.1.5. and Section 2.1.2.6). Equation 35 was used to calculate $LAI_{Equivalent}$ for every hour of the dataset as a fitting parameter to replace *LAI* in Equation 18 such that the energy balance of Equation 34 was satisfied. Daily average $LAI_{Equivalent}$ values for the dataset are shown in Figure 12 and, as seen in the figure, are significantly larger than the constant LAI value of 2.1 used in the plant evapotranspiration model. While these values do not directly represent LAI of the lettuce in the HPCF, the calculated $LAI_{Equivalent}$ values fall within the range of measured LAI for lettuce [47]. Furthermore, despite limited data on planting and harvest cycles, the results in Figure 12 coincide with cultivation data from the HPCF operator for two periods (blue shading). For the last two weeks of September, 2018, the decreasing trend in daily average

$LAI_{Equivalent}$ values coincides with a period of weekly harvest. Additionally, the increasing trend in $LAI_{Equivalent}$ values from February to May, 2019 coincides with a period of weekly planting.

$$0 = m_{w,plants} + m_{w.outdoor\ air} + m_{w,AC\ condensate} + m_{w,D\ condensate} \quad (34)$$

$$LAI_{Equivalent} = \frac{1000 \cdot m_{w,plants}}{3600 \cdot E \cdot A_{plants}} \quad (35)$$

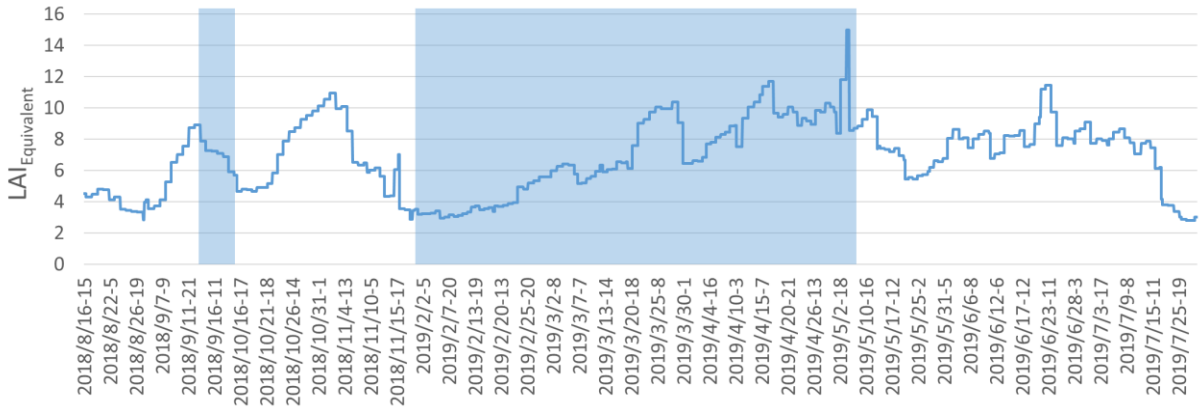

Figure 12: Calculated daily average $LAI_{Equivalent}$ values for the dataset.

While the initial physics-based model validation used measured COP values, this is not an option for models predicting future energy use of plant factories. The second validation quantified the accuracy of applying two COP scenarios to the output cooling loads of the EnergyPlus model. The first COP scenario was a constant average COP value obtained from the manufacturer specifications of the mini-split air conditioner. The second COP scenario applied COP values as a function of outdoor air temperature, as described in Section 2.1.4. This function is shown in Figure 13 in relation to measured hourly measured COP values (blue) and the manufacturer-specified COP values (red) used to obtain the function.

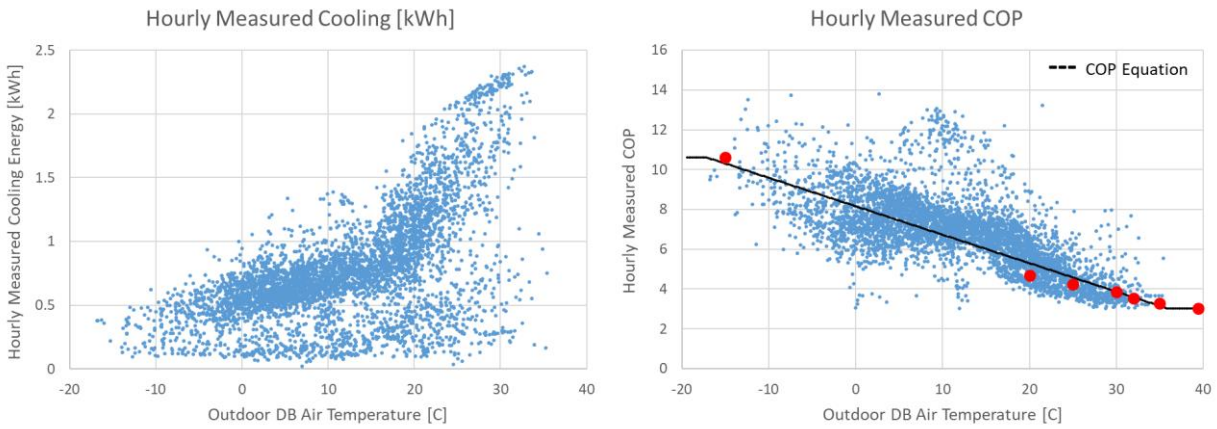

Figure 13: Hourly measured cooling energy (left) and hourly measured COP values (right) versus outdoor dry-bulb (DB) air temperature. The COP Equation as a function of outdoor air temperature is included along with the hourly measured COP values.

The results in Table 4 show that the constant COP ("Simplified") scenario has smaller NMBE error at -1% compared to -12% for the COP equation ("Recommended") scenario. However, since the results of the physics validation showed that overall the energy model underestimates the cooling load of the HPCF, these results alone cannot be used to assess the performance of the two COP sub-models. More significantly, the scenario with the COP equation scenario performs with comparable NMBE and CV(RMSE) values as the validation scenario. This is supported by the results shown in Figure 13 where it can be seen that the calculated $COP_{equation}$ values follow the hourly $COP_{measured,i}$ values with respect to outdoor air dry bulb temperature. The smaller hourly and daily CV(RMSE) values of the COP equation scenario indicate that implementing COP values as a function of outdoor air temperature may improve the reliability of the energy model in predicting cooling energy. Both COP scenarios meet the hourly whole building calibration criteria. The reliability of using these two COP scenarios to accurately predict hourly and daily cooling energy compared to the reliability of using measured COP values is further illustrated in Figure 14.

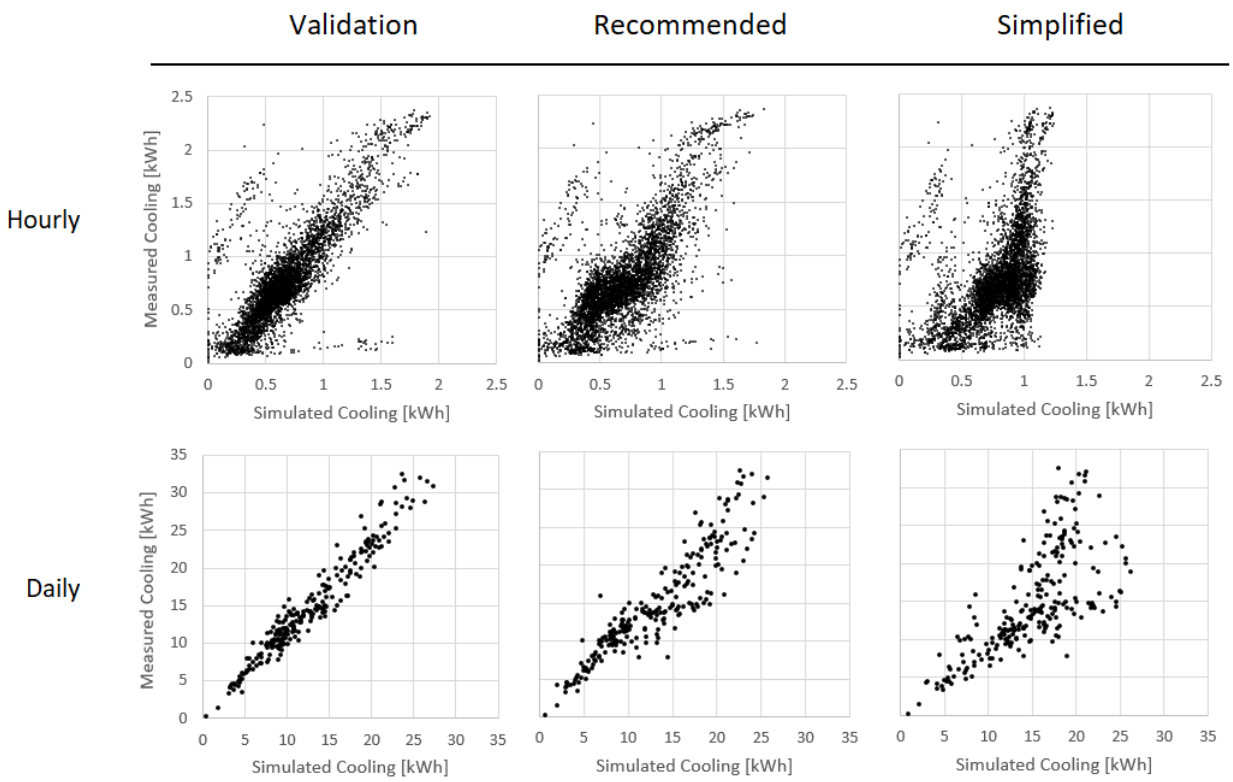

Figure 14: Comparison of measured and simulated hourly and daily cooling energy consumption using measured (Validation), equation-based (Best Practice), and constant (Standard Practice) COP values.

A subset of the hourly measurements and simulation results is shown Figure 15 illustrating that all COP scenarios of the energy model as well as the measured cooling data trail the lighting schedule of the HPCF. However, as seen in the figure, whereas the simulated cooling loads follow the lighting schedule to the hour, for this subset of the dataset hours the measured cooling loads experience a delay of approximately one hour relative to the lighting schedule. Furthermore, all three COP simulation scenarios (measured, equation, and constant) do not capture the peaks and cycling in measured cooling energy that occur throughout the lighting cycle. This accuracy in capturing high-resolutions fluctuations and peaks in hourly cooling loads is increasingly lost in the COP equation scenario and more so in the constant COP scenario.

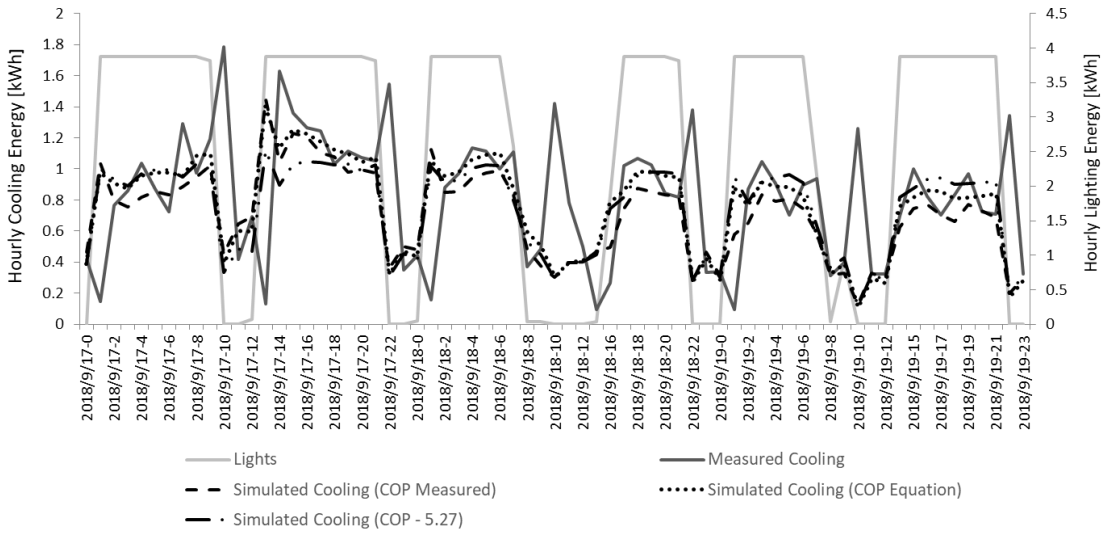

Figure 15: A three-day subset of the full dataset showing hourly measured lighting, measured cooling, and simulated cooling energy for a subset of the data. Simulated cooling energy is shown for the validation (measured COP), recommended (COP equation), and simplified (constant COP) scenarios.

3.2 Upgrade and Climate Scenarios Results

This section reviews the results of simulating various upgrade scenarios to the generic shipping container farm (template container farm) for cities in varying climates to explore the effect of upgrades on annual cooling loads and peak cooling loads. Table 5 and Table 6 summarize these results below. Notably, the simulations predicted year-round cooling in all cities showing that even in cold climates, the large internal gains in these systems require significant cooling. Independently of simulating upgrade scenarios, the "Baseline" results in Table 5 show that the greatest effect on annual cooling loads was the climate, where the hottest climate (Phoenix, AZ) resulted in more than double the annual cooling load as the coldest climate (Anchorage, AK). Among the simulated upgrade scenarios, shifting the light schedule to be off during the warmer hours of the day consistently reduced the annual cooling loads in all climates. Adding insulation to the envelope, on the other hand, reduced annual cooling loads only for the hottest climate. In the coldest climate, adding insulation to the envelope increased the annual cooling load by 10.2%.

Whereas the effects on annual cooling loads varied across the different upgrade scenarios, all upgrade scenarios reduced peak cooling loads. The one exception to this was for the coldest climate where shifting the lighting shedule increased the peak cooling load. However, this outlier can be explained by looking at the outdoor dry bulb temperatures in the Achorage TMY3 weather file at the time during which the maximum peak loads occur for the Light Shift scenario (June 14 at 18:00). This time corresponds to a day

in the weather file that not only contains the second hottest temperatures in the year, but that also maintain hotter temperatures later into the day. When the 6-hour "lights off" period terminates on June 14, the outdoor dry bulb temperatures are still increasing in temperature whereas normally at that time, the outdoor temperatures would be lower and would begin to level-off or decrease.

	Baseline	Shaded		Insulation		Lights Shift		Lights Shift + Insulation	
City	Cooling [kWh]	Cooling [kWh]	% Change	Cooling [kWh]	% Change	Cooling [kWh]	% Change	Cooling [kWh]	% Change
Boston	5373	5381	0.14	5639	4.94	5239	-2.50	5480	1.98
Phoenix	8980	9022	0.47	8877	-1.14	8650	-3.68	8523	-5.09
NewOrleans	7972	7981	0.11	8003	0.39	7751	-2.77	7757	-2.69
Denver	5495	5502	0.13	5745	4.56	5216	-5.08	5446	-0.89
Anchorage	3914	3938	0.62	4311	10.15	3845	-1.76	4212	7.62

Table 5: Effects of upgrade strategies on annual template container farm cooling loads for cities in varying climates.

	Baseline	Shaded		Insulation		Lights Shift		Lights Shift + Insulation	
City	Peak [kWh]	Peak [kWh]	% Change	Peak [kWh]	% Change	Peak [kWh]	% Change	Peak [kWh]	% Change
Boston	2.104	2.082	-1.05	2.013	-4.34	2.080	-1.16	2.066	-1.81
Phoenix	2.174	2.157	-0.81	2.100	-3.40	2.158	-0.75	2.093	-3.74
NewOrleans	2.143	2.098	-2.12	2.062	-3.78	2.134	-0.45	2.123	-0.93
Denver	2.031	2.005	-1.31	1.953	-3.85	1.937	-4.64	1.871	-7.89
Anchorage	1.208	1.198	-0.87	1.199	-0.79	1.315	8.86	1.336	10.52

Table 6: Effects of upgrade strategies on peak cooling loads for cities in varying climates

3.3 Grid Integration Results

This section reviews the results of a case study exploring variations in lighting schedules of 780 template container farms and the effects on peak energy demand of a neighborhood in Boston, MA, for the hottest day in the Boston TMY3 weather file, July 7. In this case study, as seen in Figure 16 and Table 7, adding 780 template container farms to the neighborhood with staggered lighing schedules requires an increase in peak grid capacity of 21%, or 1.4 MWh/peak hour for the neighborhood. The second scenario where all template container farm lights are turned off throughout the day requires a minimum increase in grid capacity of 15%, or 1 MWh/peak hour for the neighborhood. The results of the third scenario found that while maintaining all template container farms on the same lighitng schedule, it is possible to increase the daily photoperiod to 11 hours during the hours of the day with least neighborhood energy demand while maintaining the same required percentage increase in peak grid capacity as the second scenario.

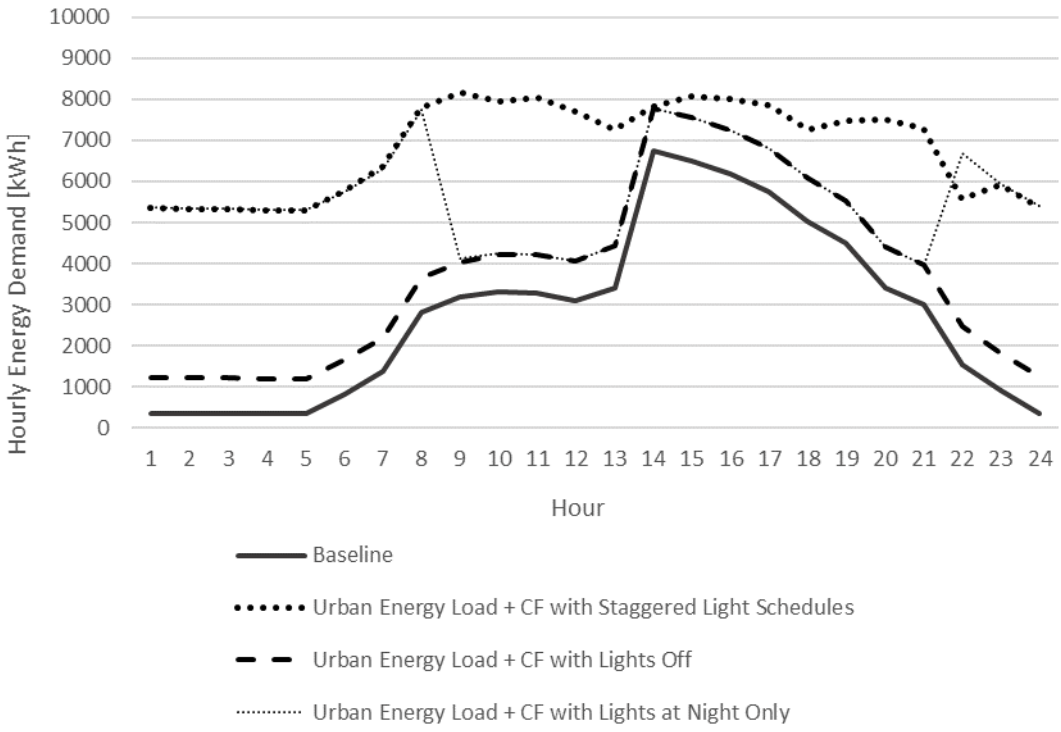

Figure 16: Hourly load curves for a Boston neighborhood during a hot summer day. The curves illustrate scenarios without container farms (baseline), with the addition of 780 container farms on a single lighting schedule, and with the addition of 780 container farms with staggered light schedules.

Lighting Scenario	Increase in Peak (%)	Increase in Peak (MWh/h)	Photoperiod (h)
Staggered Light Schedules	21	1.4	18
Lights Off	15	1.0	0
Night Lights only	15	1.0	11

Table 7: Percent increases in peak energy capacity for a Boston neighborhood with the addition of 780 container farms on a single lighting schedule, and with the addition of 780 container farms with staggered light schedules.

4 Discussion

The first objective of this research was to validate an energy model for a hydroponic container farm that takes into account plant-air interactions in the energy balance. Additionally, this research used the validated energy model in example analyses that would be of interest to owners of cities and urban planners, owners of plant factories, and utility companies. Through these example analyses, the research sought to provide an understanding of the potential to reduce conditioning loads of container farms in varying climates and the potential to reduce additional demands on urban electric grids caused by the large-scale integration of plant factories. This section comments on the results of this research in relation to these objectives.

4.1 Energy Model Validation Discussion

The results from the initial energy model validation show that including plants in building energy models of plant factories varies in importance depending on the application and scale of the energy model. Significantly, the results suggest that when conducting whole building energy models of small plant factory systems, particularly for high-level annual assessments, it is unnecessary to simulate the sensible and latent internal loads due to plants. This would reduce the complexity of such energy models as current software tools such as EnergyPlus lack components to consider plants as internal loads.

Nevertheless, as the capacity of plant factories scale and energy predictions are needed at smaller time steps, it is critical to consider plant-air interactions in the energy model whether the cooling system or whole building energy loads are being analyzed. As seen in the results of the post-processing mass balance analysis, the evapotranspiration rates in plants factories can change significantly throughout plant growth cycles, directly affecting the conditioning energy requirements. Small changes in latent and sensible loads due to plant activity could pose a significant demand on electric grid systems when compounded in large-scale plant factory systems. Additionally, the measurements of the HPCF cooling energy captured intermittent cycling and peaking that could further stress on grid capacity as plant factories scale in size.

To this objective, despite modeling considering the evapotranspiration of plants, the energy model in this research fails to accurately predict cooling energy demand at the hourly level both in magnitude (the predicted hourly cooling energy was consistently lower than the measured energy) and in behavior (the model failed to capture the cyclic behavior of the cooling system). This latter shortcoming may be

explained by inaccuracies in defining the control behavior of the HPCF cooling system. Additionally, a 60-minute timestep used in defining the energy model whereas in reality, the internal loads might fluctuate significantly at the sub-hourly level.

However, the consistent under-prediction of cooling energy may be attributed to several factors. While measured COP values were applied to the raw energy loads predicted by the EnergyPlus, as seen in the results of Figure 15, the pattern of the measured cooling demand did not always align with the simulated cooling demand. This shift in demand pattern between the measured and simulated data suggests a possible discrepancy in the alignment of measured COP values and simulated cooling loads. However, as seen in the results of the COP equation scenario when more stable COP values were applied to the raw cooling load output, this misalignment would likely have a small effect in the magnitude of the cooling energy error.

More likely, the consistent under-prediction of cooling loads may be due to inaccuracies in modeling the latent and sensible effects of plants within the HPCF. The results of the mass balance suggest an overall underestimation of evapotranspiration rates in the model. However, this may only partially explain the error because most of the calculated hourly evapotranspiration rates coincide with previously validated simulated evapotranspiration rates under comparable lighting conditions [25]. Of potential significance are the simplified methods used to calculate the sensible energy loads of the plant. These methods use the Equation 13 to calculate the sensible energy loads to satisfy the plant energy balance. However, these methods do not take into account the temperature dependence of the sensible energy flux between the plant and the container farm air. The model as is may not account for all hours during which the surface temperature of the plants is higher than the ambient temperature and the sensible heat transfer is from the plants to the air and not vice versa. This simplification may effectively overestimate the sensible cooling effect of the plants and consequently reduce the simulated cooling loads of the HPCF.

While the initial validation results illustrate the importance, complexity, and limitations of incorporating plant-air interactions in building energy models, the results of this study show that of even greater importance to the reliability of CEA energy models in predicting conditioning energy is the application of accurate COP values. The results suggest that, to the extent possible, applied COP values should be calculated for outdoor air temperature conditions that match the operating conditions of the plant factory. Furthermore, it is best to use as a function of outdoor air temperature (“Recommendation”) rather than use a constant COP values (“Simplified”). While HVAC systems vary in performance, the methods used in this research to obtain a simplified COP model as a function of outdoor air temperature are universal

whenever manufacture data are available. However, for climates in which outdoor air temperatures vary significantly from the operating conditions listed in manufacturer specifications, simplified COP models derived from manufacturer's specifications may vary significantly from the actual performance of the conditioning system (Figure 13). If only constant COP values are an option, careful attention should be given to the selection of SEER versus EER COP values depending on the outdoor air operating conditions of the plant factory. The authors further recommend that whenever possible, operators of plant factories work closely with the HVAC system manufacturers to obtain performance information for the range of outdoor air temperatures relevant to the plant factory.

Overall, the results of the energy model validation show that through the combination of incorporating plants in the energy model and modeling COP values as a function of outdoor air temperature, cities and plant factory owners can obtain a reasonable estimate of annual energy demands associated with crop cultivation. However, utility companies concerned with the capacity of the electric grid require accurate energy models at finer resolutions than annual or daily energy loads. The results in Table 4 along with the simulated hourly cooling loads in Figure 15 reveal the shortcomings of the energy model, despite incorporating plants and modeling COP as a function of outdoor air temperature, in capturing peaks and cycling of cooling energy. The limitations of this plant factory energy model indicate that, to reliably simulate conditioning energy at the hourly and even daily level, the latent and sensible effects of plant evapotranspiration must be modeled dynamically within the BPS tool and not in parallel. Furthermore, while the HPCF energy model used static values for LAI, plant factory energy models requiring accuracy at higher resolutions in time should also incorporate plant growth models to better estimate the effects of plants on conditioning loads. Finally, such large-scale and high-resolution applications would benefit from from extensive and detailed HVAC system modeling components within EnergyPlus or comparable software.

4.2 Upgrade and Climate Scenarios Discussion

The results from the first example analysis, simulating the effects on container farm cooling loads due to changes in climate and system upgrades, reveal that strategically controlling the lighting schedule to reduce internal heat gains during the warmest hours of the day has the greatest impact in reducing cooling loads. This is consistent with existing load-reduction strategies implemented by utility companies with the goal of reducing energy costs of plant factory owners. Further strategies to reduce internal heat gains of lighting loads in plant factories, as discussed by [32], may be to cycle the grow lights at a sub-hourly

schedule. However, this method should be considered alongside the effects of reduced lighting levels on plant growth.

While the remaining upgrade strategies of adding insulation and shading the container farms have minor effects on annual cooling loads, one key finding in these results is that in all but the hottest of climates, adding insulation to container farms increases annual cooling loads. These findings are counter to current trends in some requirements of plant factories. For example, commercial cannabis plant factories in Massachusetts are required to meet minimum code standards for envelope insulation [48]. According to the results of this research, these requirements would increase the annual energy demand of such systems. The results of this research show the value in providing policy makers and plant factory owners with reliable building energy models of plant factories. Furthermore, the results of this research show that refrigerated shipping containers are well insulated as designed and that design efforts of container farm manufacturers are better spent considering efficient lighting schedules rather than further insulating the containers. Finally, this study shows that even in cold climates, container farms require annual cooling. Future designs of plant factories would further benefit from developing “free cooling” strategies in cold climates.

One unexpected result from this section is the increase in annual cooling loads when shading the container farms. Analysis of hourly results shows that the addition of shading reduces hourly cooling loads during relatively hot and sunny hours but increases cooling loads during cooler darker hours, especially at night. This may be attributed to the shading surfaces reducing the radiative heat loss of the container farm during darker hours of the day. However, the relative change in cooling loads are small and the effects of shading should be further investigated.

Finally, the results from this section suggest that due to the high cooling demands of plant factories, large-scale applications of plant factories are better suited to colder climates. Particularly when examining the additional peak loads on electric grids, installing plant factories in climates with cold outdoor air temperatures would reduce the additional grid capacity required to integrate commercial agriculture in urban areas. However, as previously discussed, holistic analyses are necessary to determine the viability of plant factories for a given urban area and energy requirements alone are not sufficient to determine whether commercial urban agriculture will reduce or add to a city’s carbon emissions. This example analysis merely shows that this validated energy model can be combined with food system models to determine whether a given city, due to its climate, existing food supply methods, and food demand, would benefit from implementing commercial urban plant factories.

4.3 Grid Integration Discussion

The results from the second example analysis, integrating sufficient container farms in an urban neighborhood to meet annual vegetable demand, provide insight into how plant factory owners might work with utility companies to find a balance between maintaining sufficient levels of CEA operation while reducing added demands on electric grids. As seen in Table 7, for days in which both neighborhood and container farm system cooling demands are high, maintaining normal photoperiod levels in all plant factories will require significant increases to grid capacity, even when staggering lighting schedules to avoid the compounding effects of all container farms switching to "lights on" periods at once. As a potential remedy, the results also show that even though turning off all container farm lights throughout the day still contribute to peak energy demands of the neighborhood due to the baseline equipment and cooling requirements, this additional peak capacity is reduced. However, while switching off all container farm lights would benefit the utility company in reducing peak loads, the plant factory owners would suffer from potential crop damage as prolonged period of darkness exceeding 24 hours may fully deplete carbohydrate stores in plants [49]. These results show how this energy model, validated at the hourly level, can be used to find an intermediate solution that maintains minimum increases to peak grid capacity while maximizing CEA photoperiods. As CEA capacities continue to grow, utilities would benefit from such models to better manage demand-response programs with plant factory owners and operators.

5 Conclusion

This study successfully validated an energy model for a hydroponic container farm for hourly predictions of whole building energy in compliance with [30]. The results of the study show that the limitations of plant factory energy models are significantly influenced by errors in modeling plant-air interactions and COP values for the conditioning system. As a solution, this research suggests a simplified and universal method for modeling COP as a function of outdoor temperature with comparable results to the energy model validation. Using the template energy model for a container farm, this research demonstrated the potential in developing robust tools to assess the feasibility of implementing large-scale plant factories in urban areas. As shown in this research, this is not only crucial to understanding the overall impact on carbon emissions in an urban area, but also to planning the integration of such systems within the infrastructure of cities. This research showed that insulation is counterproductive to reducing annual energy loads in mild and cold climates. Additionally, this research shows the importance of reducing lighting loads while maintaining crop yield, both for reducing cooling and total energy demand. These results encourage those regulating plant factories to consider these buildings as a new category in building codes and regulations. Finally, this research reveals potential tradeoffs that plant factory owners and utility companies will have to make when incorporating large plant factories in electric grids.

References

[1] H. Coninck *et al.*, “2018: Strengthening and Implementing the Global Response,” in *Global Warming of 1.5°C. An IPCC Special Report on the impacts of global warming of 1.5°C above pre-industrial levels and related global greenhouse gas emission pathways, in the context of strengthening the global response to the threat of climate change, sustainable development, and efforts to eradicate poverty*, Masson-Delmotte, V., P. Zhai, H.-O. Pörtner, D. Roberts, J. Skea, P.R. Shukla, A. Pirani, W. Moufouma-Okia, C. Péan, R. Pidcock, S. Connors, J.B.R. Matthews, Y. Chen, X. Zhou, M.I. Gomis, E. Lonnoy, T. Maycock, M. Tignor, and T. Waterfield (eds.), In press.

[2] City of Boston, “City of Boston Greenhouse Gas Emissions Inventory (2005-2017),” 2019. Accessed: Jul. 21, 2020. [Online]. Available: https://www.boston.gov/departments/environment/bostons-carbon-emissions.

[3] L. Zhang, G. Liu, and Y. Qin, “Multi-scale integrated assessment of urban energy use and CO2 emissions,” *J. Geogr. Sci.*, vol. 24, no. 4, pp. 651–668, Aug. 2014, doi: 10.1007/s11442-014-1111-5.

[4] P. J. Marcotullio, A. Sarzynski, J. Albrecht, and N. Schulz, “A Top-Down Regional Assessment of Urban Greenhouse Gas Emissions in Europe,” *AMBIO*, vol. 43, no. 7, pp. 957–968, Nov. 2014, doi: 10.1007/s13280-013-0467-6.

[5] S. Vermeulen, B. M. Campbell, and J. Ingram, “Climate Change and Food Systems,” *Annual Review of Environment and Resources*, vol. 37, pp. 195–222, Oct. 2012, doi: 10.1146/annurev-environ-020411-130608.

[6] F. Zabel, B. Putzenlechner, and W. Mauser, “Global agricultural land resources--a high resolution suitability evaluation and its perspectives until 2100 under climate change conditions,” *PloS one*, vol. 9, no. 9, p. e107522, Sep. 2014, doi: 10.1371/journal.pone.0107522.

[7] M. Kulak, A. Graves, and J. Chatterton, “Reducing greenhouse gas emissions with urban agriculture: A Life Cycle Assessment perspective,” *Landscape and Urban Planning*, vol. 111, pp. 68–78, Mar. 2013, doi: 10.1016/j.landurbplan.2012.11.007.

[8] B. Goldstein, M. Hauschild, J. Fernández, and M. Birkved, “Urban versus conventional agriculture, taxonomy of resource profiles: a review,” *Agron. Sustain. Dev.*, vol. 36, no. 1, p. 9, Jan. 2016, doi: 10.1007/s13593-015-0348-4.

[9] K. Benis and P. Ferrão, “Potential mitigation of the environmental impacts of food systems through urban and peri-urban agriculture (UPA) – a life cycle assessment approach,” *Journal of Cleaner Production*, vol. 140, pp. 784–795, Jan. 2017, doi: 10.1016/j.jclepro.2016.05.176.

[10] F. Martellozzo, J.-S. Landry, D. Plouffe, V. Seufert, P. Rowhani, and N. Ramankutty, “Urban agriculture: a global analysis of the space constraint to meet urban vegetable demand,” *Environ. Res. Lett.*, vol. 9, no. 6, p. 064025, May 2014, doi: 10.1088/1748-9326/9/6/064025.

[11] T. Kozai, “Resource use efficiency of closed plant production system with artificial light: Concept, estimation and application to plant factory,” *Proceedings of the Japan Academy. Series B, Physical and biological sciences*, vol. 89, pp. 447–461, Dec. 2013, doi: 10.2183/pjab.89.447.

[12] T. Kozai, “Plant Factory in Japan - Current situation and perspectives,” *Chronica horticulturae*, vol. 53, pp. 8–11, Jan. 2013.
[13] S. W. Van Ginkel, T. Igou, and Y. Chen, “Energy, water and nutrient impacts of California-grown vegetables compared to controlled environmental agriculture systems in Atlanta, GA,” *Resources, Conservation and Recycling*, vol. 122, pp. 319–325, Jul. 2017, doi: 10.1016/j.resconrec.2017.03.003.
[14] L. Graamans, E. Baeza, A. van den Dobbelsteen, I. Tsafaras, and C. Stanghellini, “Plant factories versus greenhouses: Comparison of resource use efficiency,” *Agricultural Systems*, vol. 160, pp. 31–43, Feb. 2018, doi: 10.1016/j.agsy.2017.11.003.
[15] K. Benis and P. Ferrao, “Commercial farming within the urban built environment – Taking stock of an evolving field in northern countries,” *Global Food Security*, vol. 17, pp. 30–37, Jun. 2018, doi: https://doi.org/10.1016/j.gfs.2018.03.005.
[16] W. Goodman and J. Minner, “Will the urban agricultural revolution be vertical and soilless? A case study of controlled environment agriculture in New York City,” *Land Use Policy*, vol. 83, pp. 160–173, Apr. 2019, doi: 10.1016/j.landusepol.2018.12.038.
[17] J. Farfan, A. Lohrmann, and C. Breyer, “Integration of greenhouse agriculture to the energy infrastructure as an alimentary solution,” *Renewable and Sustainable Energy Reviews*, vol. 110, pp. 368–377, Aug. 2019, doi: 10.1016/j.rser.2019.04.084.
[18] S. Potlog, C. Gherghina, and A. Vintea, “Containerized modular data centers powered by wind farms,” in *2015 7th International Conference on Electronics, Computers and Artificial Intelligence (ECAI)*, Jun. 2015, p. P-117-P-120, doi: 10.1109/ECAI.2015.7301264.
[19] Z. Sun, H. Mei, and R. Ni, “Overview of Modular Design Strategy of the Shipping Container Architecture in Cold Regions,” *IOP Conf. Ser.: Earth Environ. Sci.*, vol. 63, p. 012035, May 2017, doi: 10.1088/1755-1315/63/1/012035.
[20] K. Benis, C. F. Reinhart, and P. Ferrao, “Building Integrated Agriculture (BIA) in Urban Context: Testing a Simulation-Based Decision Support Workflow,” in *Proceedings of the 15th IBPSA Conference*, San Francisco, CA, Aug. 2017, pp. 1798–1807, doi: https://doi.org/10.26868/25222708.2017.479.
[21] K. Benis, C. F. Reinhart, and P. Ferrao, “Development of a simulation-based decision support workflow for the implementation of building-integrated agriculture (BIA) in urban contexts,” *Journal of Cleaner Production*, vol. 147, pp. 589–602, Mar. 2017, doi: 10.1016/j.jclepro.2017.01.130.
[22] MIT Sustainable Design Lab, “Harvest.” https://urbanfoodprints.com/#/.
[23] E. Iddio, L. Wang, Y. Thomas, G. McMorrow, and A. Denzer, “Energy efficient operation and modeling for greenhouses: A literature review,” *Renewable and Sustainable Energy Reviews*, vol. 117, p. 109480, Jan. 2020, doi: 10.1016/j.rser.2019.109480.
[24] F. Golzar, N. Heeren, S. Hellweg, and R. Roshandel, “A novel integrated framework to evaluate greenhouse energy demand and crop yield production,” *Renewable and Sustainable Energy Reviews*, vol. 96, pp. 487–501, Nov. 2018, doi: 10.1016/j.rser.2018.06.046.
[25] L. Graamans, A. van den Dobbelsteen, E. Meinen, and C. Stanghellini, “Plant Factories; crop transpiration and energy balance,” *Agricultural Systems*, vol. 153, pp. 138–147, May 2017, doi: https://doi.org/10.1016/j.agsy.2017.01.003.
[26] M.-H. Talbot and D. Monfet, “Impact des plantes sur les charges d’un espace d’agriculture intégré au bâtiment : Implantation d’un modèle de plantes,” May 2018.

[27] G. Kokogiannakis and P. Cooper, “Evaluating the environmental performance of indoor plants in buildings,” Dec. 2015.
[28] K. Harbick and L. D. Albright, “Comparison of energy consumption: greenhouses and plant factories,” *Acta Hortic.*, no. 1134, pp. 285–292, May 2016, doi: 10.17660/ActaHortic.2016.1134.38.
[29] R. V. Ward, R. Choudhary, C. Cundy, G. Johnson, and A. McRobie, “Simulation of plants in buildings; incorporating plant-Air interactions in building energy simulation,” 2015.
[30] American Society of Heating, Refrigerating and Air-Conditioning Engineers, “ASHRAE Guideline 14-2014: Measurement of Energy, Demand, and Wate Savings.” 2014.
[31] Contenedores y Embalajes Normalizados S.A., “40’HC REEFER COLD STORAGE TECHNICAL SPEC. BULLBOX.” Oct. 2017.
[32] D. Chickarello, M. Agyemang, A. S. Gill, J. D. Summers, C. J. Turner, and J. R. Wagner, “Extraterrestrial Farming with the Leafy Green Machine – LED Performance Testing,” presented at the 47th International Conference on Environmental Systems, Charleston, SC, Jul. 2017.
[33] D. Katzin, S. van Mourik, F. Kepkes, and E. J. van Henten, “GreenLight – An open source model for greenhouses with supplemental lighting: Evaluation of heat requirements under LED and HPS lamps,” *Biosystems Engineering*, vol. 194, pp. 61–81, Jun. 2020, doi: https://doi.org/10.1016/j.biosystemseng.2020.03.010.
[34] NREL, “1.13.4 Group - Internal Gains, Lights,” in *EnergyPlus Version 9.1.0 Documentation, Input Output Reference*, 2019, pp. 480–490.
[35] Therma-Stor LLC, “Santa Fe Classic Dehumidifier Datasheet, Performance and Technical Specs.” Part No. 4029700, Accessed: Nov. 19, 2019. [Online].
[36] NREL, “19.6.9 Zone Air DX Dehumidifier,” in *EnergyPlus Version 9.1.0 Documentation, Engineering Reference*, 2019, pp. 1584–1590.
[37] J. A. Winkler, D. Christensen, and J. Tomerlin, “Measured Performance of Residential Dehumidifiers Under Cyclic Operation,” National Renewable Energy Laboratory, Technical Report NREL/TP-5500-61076, 2014.
[38] D. Katzin, S. van Mourik, F. Kempkes, and E. J. van Henten, “GreenLight – An open source model for greenhouses with supplemental lighting: Evaluation of heat requirements under LED and HPS lamps,” *Biosystems Engineering*, vol. 194, pp. 61–81, Jun. 2020, doi: 10.1016/j.biosystemseng.2020.03.010.
[39] J. L. Monteith, “Evaporation and environment,” *Symposia of the Society for Experimental Biology*, vol. 19, pp. 205–234, 1965.
[41] N. Katsoulas and C. Stanghellini, “Modelling Crop Transpiration in Greenhouses: Different Models for Different Applications,” *Agronomy*, vol. 9, no. 7, p. 392, Jul. 2019, doi: 10.3390/agronomy9070392.
[42] H.-H. Kim, G. D. Goins, R. M. Wheeler, and J. C. Sager, “Stomatal Conductance of Lettuce Grown Under or Exposed to Different Light Qualities,” *Ann Bot*, vol. 94, no. 5, pp. 691–697, Nov. 2004, doi: 10.1093/aob/mch192.
[43] McNeel, “Rhinoceros 6.0,” 2019. https://www.rhino3d.com/.
[44] Daikin Industries, Ltd., “Split Type Air Conditioners - Cooling Only / Heat Pump - SEER 18 Models, FTK(X)-N Series.” EDUS041502.
[45] C. Reinhart, T. Dogan, J. Jakubiec, T. Rakha, and A. Sang, “UMI - An urban simulation environment for building energy use, daylighting and walkability,” presented at the

Proceedings of BS 2013: 13th Conference of the International Building Performance Simulation Association, Jan. 2013.
[46] C. Cerezo, T. Dogan, and C. Reinhart, “Towards standarized building properties template files for early design energy model generation,” Jan. 2014.
[47] F. Tei, A. Scaife, and D. P. Aikman, “Growth of Lettuce, Onion, and Red Beet. 1. Growth Analysis, Light Interception, and Radiation Use Efficiency,” *Ann Bot*, vol. 78, no. 5, pp. 633–643, Nov. 1996, doi: 10.1006/anbo.1996.0171.
[48] State of Massachusetts, “935 CMR 500.120(11)(a) Adult Use of Marijuana,” Code of Massachusetts Regulations, 2018.
[49] C. Gary, P. Baldet, N. Bertin, C. Devaux, M. Tchamitchian, and P. Raymond, “Time-course of Tomato Whole-plant Respiration and Fruit and Stem Growth During Prolonged Darkness in Relation to Carbohydrate Reserves,” *Annals of Botany*, vol. 91, no. 4, p. 429, 2003.